Monthly Notices of the ROYAL ASTRONOMICAL SOCIETY

MNRAS **506,** 4302–4320 (2021) https://doi.org/10.1093/mnras/stab1947
Advance Access publication 2021 July 9

The impact of physical processes on the estimation of the ages of asteroid families

A. Dell'Oro [1]★ J. Boccenti,[2] F. Spoto,[3] P. Paolicchi[2] and Z. Knežević [4]

[1] *INAF – Osservatorio Astrofisico di Arcetri, Largo E. Fermi 5, I-50125 Firenze, Italy*
[2] *Department of Physics, University of Pisa, Largo Pontecorvo 3, I-56127 Pisa, Italy*
[3] *Harvard-Smithsonian Center for Astrophysics, 60 Garden St, MS 15, Cambridge, MA 02138, USA*
[4] *Serbian Academy of Sciences and Arts, Kneza Mihaila 35, 11000 Belgrade, Serbia*

Accepted 2021 June 29. Received 2021 June 29; in original form 2021 March 31

ABSTRACT

One of the methods used to estimate the ages of the asteroid families is based on the interpretation of the distribution of the sizes versus orbital semimajor axes of their members as the result of their post-formation dynamical evolution. The fundamental hypothesis is that the present distribution of the semimajor axes is essentially the product of the Yarkovsky effect. On the other hand, the observable features of the asteroid families can be affected by several physical and dynamical processes. In this paper, we discuss the role of: (1) the initial distribution of the ejection velocities at the time of the primordial break-up event; (2) the possible correlations between the family members ejection direction and the orientation of the rotational axis (which the direction of the Yarkovsky semimajor axis drift depends on); (3) the gravitational reaccumulation of the parent body fragments during the ballistic phase of the formation process; and (4) the collisional re-orientation of the spin axes during the post-formation evolution phase. We show how each of these mechanisms affects the determination of the ages of the asteroid families, and what additional information can be inferred regarding some aspects of the collisional evolution of the rotation axes.

Key words: minor planets, asteroids: general.

1 INTRODUCTION

The dynamical effect on the asteroid orbits due to the absorption of the solar radiation, the body differential heating, and subsequent infrared re-emission, known as Yarkovsky effect (Bottke et al. 2002), has played a key role in the last two decades in the study of the evolution of the Main Belt Asteroids and the origin of the Near-Earth Asteroids. In particular the importance of this mechanism for the interpretation of the structure of the asteroid families has been recognized two decades ago (Bottke et al. 2001), and it has been exploited in order to improve the methods of families identification (Bolin et al. 2017). The Yarkovsky effect also offers an opportunity to estimate the age of the asteroid families. The perturbations on an asteroid orbit caused by the Yarkovsky effect, and in particular the secular drift rate of the semimajor axis, is inversely proportional to the size of body. Under the assumption that the Yarkovsky effect played a dominant role in the post-formation orbital evolution of an asteroid family, plotting the absolute magnitude H of the family members against their proper semimajor axes a we should obtain a triangular structure where the dispersion of the semimajor axes increases with the absolute magnitude. As the dispersion of the semimajor axes is directly related to the time elapsed since the primordial break-up producing the family, its a–H plot allows us to retrieve indirect information about the age of the family (Farinella & Vokrouhlický 1999; 2006a). A slightly different approach has been proposed by Milani et al. (2014) and Spoto, Milani & Knezevic (2015) consisting in the analysis of the structure of the asteroid families in the plane where the diameters $1/D$ of the members are plotted against their semimajor axes. The typical V-shape structure of the asteroid families in the plane $1/D$ versus a appears as the natural by-product of the dependence of the Yarkovsky drift rate of the semimajor axis on the inverse of the diameter. A geometrical analysis of the V-shape structure together with an independent evaluation of the Yarkovsky drift rate makes possible the estimation of the asteroid family ages.

Although the basic idea is simple, the determination of the ages of the real asteroid families is not a trivial procedure. In addition to some technical problems in the analysis of the V-shapes and to the different sources of uncertainty coming from the observational data, the assumption that the Yarkovsky effect alone dominates the evolution of the V-shape diagram and its present structure could be simplistic. The authors of the method have already warned that the initial orbital dispersion of young asteroid families can introduce a non-negligible error in the family age determination. Indeed young asteroid families can give us the opportunity to obtain important information about the poorly known primordial break-up velocity fields, before their signatures are confused with the post-formation evolution due to the Yarkovsky effect (Vokrouhlický et al. 2006b; Bolin et al. 2018; Carruba, Vokrouhlický & Novaković 2018).

In this paper, we want to discuss the role of mechanisms other than the Yarkovsky effect in the evolution of the asteroid family V-shapes and their impact on the age determination. To do this we have developed a synthetic model of the V-shape of the asteroid families including different features. The model is described in Section 2. In

★ E-mail: aldo.dellorо@inaf.it

this model, we followed a semi-analytical approach based neither on simulations of break-up process relying on a detailed description of the fragmentation physics nor on direct numerical orbital integration. We tried to implement a realistic description of the relevant physical and dynamical processes but with a wide flexibility in order to explore several aspects of the problem. After a detailed description of the model, a summary of the procedure used to estimate the age of asteroid families is presented in Section 3. Moreover, in this section some important technical details are discussed in order to apply the method to simulated asteroid families. The results of a series of simulations performed in order to test the effect of each individual physical mechanism, one at a time, will be discussed in Section 4. Finally, in Section 5 we give some conclusions of this work.

2 ASTEROID FAMILY MODEL

In this section, we will describe in detail the numerical model used to simulate the formation and evolution of a generic asteroid family. The goal of this model is not to reproduce all the details of such a complex process but only to highlight the relevant features impacting the age determination. In particular, the model does not include a numerical integration of the member orbits taking into account at the same time planetary perturbations and the Yarkovsky acceleration. Such computation is beyond the scope of this work.

The model is composed of two separate modules: one devoted to the computation of the initial values of the orbital elements of the family members, and the other pertaining to the evolution of their semimajor axes. In both cases, by orbital elements we mean *synthetic proper* orbital elements (Knežević & Milani 2000, 2003), assuming that the original difference among proper elements just after the formation of the family is related to the final velocities of the fragments at infinity through Gauss' equations and the orbital circumstances of the impact (Brouwer 1951; Zappalà et al. 1996).

2.1 Break-up simulation

Beside asteroid size, the Yarkovsky effect, both in diurnal and seasonal versions, depends on the orientation of the rotational axis, and more precisely is proportional to $\cos\phi$ and $\sin^2\phi$, respectively, where ϕ is the obliquity of the spin axis, the angle, from 0 to π, between the asteroid polar axis and the normal to its orbital plane (Farinella, Vokrouhlický & Hartmann 1998; Vokrouhlický 1999). The obliquity basically determines the direction of the semimajor axis drift. In diurnal effect, prograde rotations ($0 \leq \phi < \pi/2$) cause semimajor axis to increase, while retrograde rotations ($\pi/2 < \phi \leq \pi$) give rise to semimajor axis decrease. For this reason, the break-up model should include a description of the distribution of the initial spin axes, and possible correlations between spin axes and ejection velocities. Avoiding to enter into the complex details of the break-up physics of asteroid-sized bodies, we want to define our model in a way as simple as possible but with the necessary flexibility to describe some peculiarities of the geometry of the spin–velocity field. For the purpose of this paper (as it will be clearer later), we neglect the description of the size distribution of the fragments, focusing on the relationship among size, ejection velocity, and spin axis.

The starting point of our model is a symmetry axis of the spin–velocity field defined by a unit vector $\hat{\boldsymbol{k}}$. From the physical point of view, the vector $\hat{\boldsymbol{k}}$ is related to the impact direction. Neglecting the initial distribution of the fragments inside the parent body, we define a simple general rule to assign an *ejection velocity* vector $\boldsymbol{v}_{\rm ej} = v_{\rm ej}\hat{\boldsymbol{v}}$ to a given fragment (supposed spherical) with diameter D, where $\hat{\boldsymbol{v}}$ is a radial unit vector. In our model, this procedure can be completely random or not. We denote by x_M a random variate with Maxwellian parent distribution with mean value equal to 1. The magnitude $v_{\rm ej}$ of the vector is given by

$$|\boldsymbol{v}_{\rm ej}| = v_m(D)[1 + m_v(x_M - 1)], \tag{1}$$

where m_v is an integer number the value of which can be 0 or 1 only. If $m_v = 0$, all fragments with diameter D have the same velocity $v_m(D)$, while if $m_v = 1$ the ejection velocity of a fragment with diameter D is a Maxwellian random variable with mean value equal to $v_m(D)$. The parameter $v_m(D)$ is related to the diameter through a simple power-law function:

$$v_m(D) = v_0 \left(\frac{D}{D_0}\right)^{-\beta}, \tag{2}$$

where v_0 is the mean ejection velocity of the fragments with diameter D_0. We implemented the expression (1) in order to ensure maximum flexibility to the model, choosing from one run to another whether to adopt a Maxwellian distribution or a deterministic approach. For reasons that will be discussed later, in this work we limit ourselves to the deterministic case $m_v = 0$. The unit vector $\hat{\boldsymbol{v}}$, which describes the ejection direction of the fragment, is randomly chosen with isotropic distribution. In order to describe the case of cratering ejections, a limit value η_v for the angle between $\hat{\boldsymbol{v}}$ and the symmetry axis $\hat{\boldsymbol{k}}$ can be introduced, assuming that only fragments $\hat{\boldsymbol{v}} \cdot \hat{\boldsymbol{k}} > \cos\eta_v$ exist. The case $\eta_v = \pi$ corresponds to a completely spherical and isotropic fragmentation.

While D_0 is only a reference value of the fragment sizes, v_0 and β are physical parameters of the model. We will explore the impact of different values of v_0 on the family age determination. For what concerns the exponent, some pieces of evidence suggest that the value of β should be of the order of 1 (Cellino et al. 1999; Brož & Morbidelli 2013), as implied also by the analysis of very young asteroid families (Nesvorný et al. 2002; Bolin et al. 2018), or suggested by the distribution of the proper inclinations of the more evolved Koronis family (Carruba, Nesvorný & Aljbaae 2016). On the other hand, precise and conclusive evaluations do not exist. In this work, we limit ourselves to the case $\beta = 1$.

In order to include in a simple way the effect of the gravitational reaccumulation, we assume that, at the end of the ballistic phase of the family formation, the final fragment velocity, that for clarity we will call *exit velocity* to distinguish it from the *ejection velocity*, is reduced by an amount depending on the effective escape velocity $v_{\rm esc}$. More precisely, the exit velocity of the fragment is

$$\begin{aligned} v &= \sqrt{v_{\rm ej}^2 - v_{\rm esc}^2} \quad (v_{\rm ej} > v_{\rm esc}) \\ v &= 0 \quad (v_{\rm ej} < v_{\rm esc}), \end{aligned} \tag{3}$$

while the direction $\hat{\boldsymbol{v}}$ remains the same for both the ejection and exit velocity. We simply assume that all fragments with ejection velocity below the $v_{\rm esc}$ value fall back on the largest remnant. A similar approach has been already exploited in the context of the simulation of the collisional evolution of the asteroids size distribution (Petit & Farinella 1993; O'Brien & Greenberg 2005). The value of the effective escape velocity $v_{\rm esc}$ is a free parameter of the model. Different methods have been developed and tested in order to define precisely the concept of mean or effective escape velocity (Farinella et al. 1988; D'Abramo, Dell'Oro & Paolicchi 1999). In our model, we prefer, for reasons that will be clear soon, not to refer directly to the value of $v_{\rm esc}$ but rather to follow another approach. The condition $v_{\rm ej} > v_{\rm esc}$ entails that only fragments with $D < D_{\rm lim}$ do not reaccumulate on the largest remnant, thus contributing to the membership of the

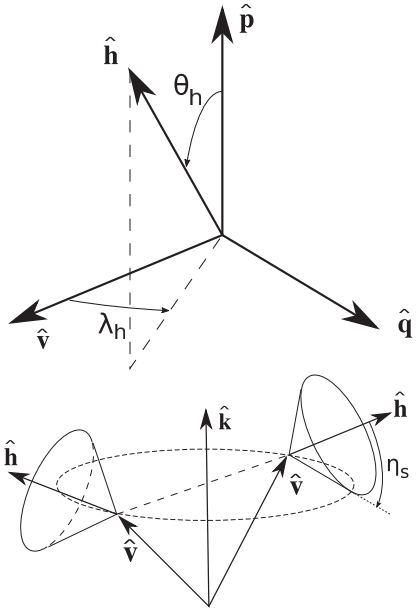

Figure 1. Auxiliary unit vectors used to describe the direction of the spin. At the top, the orthonormal axes, defined for a particular fragment, with respect to the direction $\hat{\boldsymbol{h}}$ of the mean spin axis is defined: the unit vector $\hat{\boldsymbol{v}}$ along the ejection velocity, the unit vector $\hat{\boldsymbol{p}}$ normal to the plane containing $\hat{\boldsymbol{v}}$ and the global symmetry axis of the spin–velocity field $\hat{\boldsymbol{k}}$, and $\hat{\boldsymbol{q}} = \hat{\boldsymbol{p}} \times \hat{\boldsymbol{v}}$. The spin direction for a particular fragment is randomly generated inside a cone of semi-aperture η_s around $\hat{\boldsymbol{h}}$ (bottom).

asteroid family, where $D_{\rm lim}$ is

$$D_{\rm lim} = D_0 \left(\frac{v_0}{v_{\rm esc}} \right)^{1/\beta} . \tag{4}$$

Because of the stochastic nature of the ejection velocity generation, the value $D_{\rm lim}$ is not a sharp limit, and fragments slightly larger than $D_{\rm lim}$ can escape on independent orbits, while fragments slightly smaller than $D_{\rm lim}$ can fall back contributing to the formation of the largest remnant.

In our model, we use $D_{\rm lim}$ as the parameter controlling the reaccumulation process instead of $v_{\rm esc}$, because the former is directly related to the geometrical properties of the V-shape of the asteroid family, as shown in Section 4.3, and analytically discussed in Appendix B. The two model parameters v_0 and $D_{\rm lim}$ together control the initial extension of the V-shape.

For what concerns the rotational properties of the fragment, the spin axis is defined with reference to the ejection velocity vector and the symmetry axis. For the particular fragment, a set of three orthonormal axes is defined (Fig. 1). This set is composed by $\hat{\boldsymbol{v}}$, the unit vector $\hat{\boldsymbol{p}}$ normal to the plane containing $\hat{\boldsymbol{v}}$ and $\hat{\boldsymbol{k}}$:

$$\hat{\boldsymbol{p}} = \frac{\hat{\boldsymbol{k}} \times \hat{\boldsymbol{v}}}{|\hat{\boldsymbol{k}} \times \hat{\boldsymbol{v}}|} \tag{5}$$

and the unit vector $\hat{\boldsymbol{q}}$:

$$\hat{\boldsymbol{q}} = \hat{\boldsymbol{p}} \times \hat{\boldsymbol{v}} \tag{6}$$

It is worthwhile to note that, since we have assumed that the ejection and the exit velocity of a fragment have the same direction, in the definition of the unit vectors $\hat{\boldsymbol{p}}$ and $\hat{\boldsymbol{q}}$ it is irrelevant whether we use the ejection or the exit velocity. This is important because any correlation between the components of the spin vector and those of the ejection velocity holds for the exit velocity too. At this point, a unit vector $\hat{\boldsymbol{h}}$ is defined with respect to the set $(\hat{\boldsymbol{v}}, \hat{\boldsymbol{q}}, \hat{\boldsymbol{p}})$:

$$\hat{\boldsymbol{h}} = (\sin\theta_h \cos\lambda_h)\hat{\boldsymbol{v}} + (\sin\theta_h \sin\lambda_h)\hat{\boldsymbol{q}} + (\cos\theta_h)\hat{\boldsymbol{p}} \tag{7}$$

The unit vector $\hat{\boldsymbol{s}}$ describing the spin axis orientation is isotropically generated with the constraint that the angle between $\hat{\boldsymbol{s}}$ and $\hat{\boldsymbol{h}}$ is smaller than a limit value η_s between 0 and π. In other words, the unit vector $\hat{\boldsymbol{h}}$ is the mean direction, and the axis of symmetry, of the probability distribution of the spin axis direction of the particular fragment.

The two angles θ_h and λ_h are free parameters not depending on the ejection velocity of the fragment. In this way, the orientation of the unit vector $\hat{\boldsymbol{h}}$ is cylindrically symmetric with respect to the fundamental symmetry axis $\hat{\boldsymbol{k}}$ (Fig. 1). In the case $\eta_s = \pi$, the spin axis is completely randomized with no correlation with the velocity vector. On the contrary, if $\eta_s = 0$ the spin axis is rigidly 'polarized' along $\hat{\boldsymbol{h}}$. In this case, according to the values of the angles θ_h and λ_h, different kinds of correlation arise between the components of $\hat{\boldsymbol{s}}$ and the components of $\hat{\boldsymbol{v}}$, as discussed in Section 4.2 and Appendix A.

The magnitude s of the spin vector is computed in a similar way to what was done for the velocity. More precisely $s = 2\pi/P$, where P is the rotational period. The value of s is a random variate with Maxwellian parent distribution the mean value of which is

$$s_m(D) = s_0 \left(\frac{D}{D_0} \right)^{-\gamma} , \tag{8}$$

where s_0 is the mean rotation angular frequency of the members with size D_0, and the exponent γ is free parameters. In this work, we adopt a simplified model for the evolution of the proper semimajor axis due to the Yarkovsky effect (see Section 2.3), where the rate of variation of the semimajor axis does not depend explicitly on the rotation period of the asteroid. This means that the simulated evolution of the family is not affected by the choice of the values of γ and s_0 but it depends on the spin axes orientation distribution only, or in other words it depends on θ_h, λ_h, and η_s. We keep the general approach of equation (8) for further investigations.

2.2 Initial dynamical family

Once we generated the list, the random triples $(D_k, \boldsymbol{v}_k, \boldsymbol{s}_k)$, where D_k is the diameter, $\boldsymbol{v}_k$ the exit velocity (the velocity at infinity after the reaccumulation phase), and $\boldsymbol{s}_k$ is the spin vector of the k-th member, the corresponding orbital elements of the initial dynamical family are computed from the vectors $\boldsymbol{v}_k$. The initial proper orbital elements of the parent body are supposedly known as free parameters: the semimajor axis a_{pb}, the eccentricity e_{pb}, the inclination I_{pb}, the longitude of the ascending node Ω_{pb}, the argument of the pericentre ω_{pb}, and the true anomaly f_{pb}, the latter three at the epoch of the break-up. The list of the initial orbital elements a_k, e_k, and I_k of the k-th fragment can be computed by means of the Gauss' equations, if the size of the exit velocities v_k are small compared to the orbital velocity of the parent body (Zappalà et al. 1996), or using the exact formulas of the two-body problem. The position vector $\boldsymbol{r}_{pb}$ and the orbital velocity $\boldsymbol{v}_{pb}$ of the parent body at the moment of the break-up are computed from its orbital elements. Then, the initial position and orbital velocity of the k-th fragment are $\boldsymbol{r}_{pb}$ and $\boldsymbol{v}_{pb} + \boldsymbol{v}_k$, respectively, from which the corresponding orbital elements are computed. In any case the assumption is that the exit velocities $\mathbf{v}_k$ are defined in the reference system of the parent body, physically defined as the barycentre of the system target-projectile in the collision event.

Before performing the transformation from exit velocities to orbital elements, a rotation of the spin–velocity field is performed

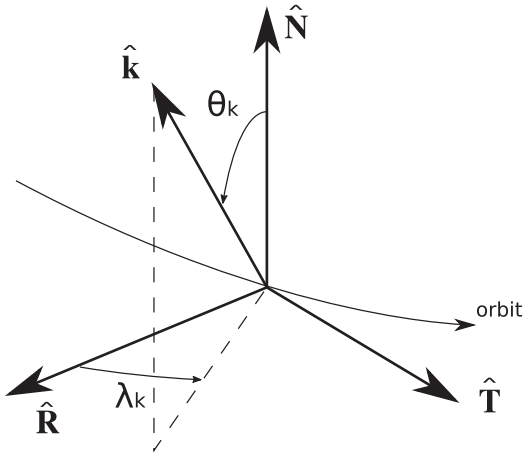

Figure 2. Orientation of the spin–velocity field symmetry axis $\hat{\mathbf{k}}$, with respect to the Gauss orthonormal basis.

in order to take into account the geometry of the impact. Because of the previously defined field is symmetric with respect to rotations about the symmetry axis $\hat{\boldsymbol{k}}$, the orientation of the field in space is completely defined by the orientation of the unit vector $\hat{\boldsymbol{k}}$, that in turn can be expressed by two angles. With respect to the co-moving Gauss orthonormal axes (Murray & Dermott 1999) $\hat{\boldsymbol{R}}$ (radial unit vector from the Sun), $\hat{\boldsymbol{N}}$ (unit vector along the orbital angular momentum, normal to the orbit plane), and $\hat{\boldsymbol{T}} = \hat{\boldsymbol{N}} \times \hat{\boldsymbol{R}}$ (transverse unit vector), the unit vector $\hat{\boldsymbol{k}}$ is defined by the two angles θ_k and λ_k such that:

$$\boldsymbol{k} = (\sin\theta_k \cos\lambda_k)\boldsymbol{R} + (\sin\theta_k \sin\lambda_k)\boldsymbol{T} + (\cos\theta_k)\boldsymbol{N} \tag{9}$$

as shown in Fig. 2.

The final output of this stage is the list of the sets of diameter, orbital elements, and spin vector (D_k, a_k, e_k, I_k, Ω_k, $\mathbf{s}_k$) for each body, even if we are interested only in the structure and evolution of the a-1/D diagram. The initial obliquity ϕ_k is computed from the spin axis $\mathbf{s}_k$, the orbital inclination I_k, and the longitude of ascending node Ω_k. The final set of parameters used for the simulation of the evolution of the V-shape, as described in Section 2.3, is composed by the values of diameter, semimajor axis, eccentricity, and obliquity (D_k, a_k, e_k, ϕ_k) for each member of the family.

2.3 Post-formation evolution

Following the approach of Milani et al. (2014), we assume that the evolution of the semimajor axis due to the Yarkovsky effect is described by the following expression:

$$\frac{\mathrm{d}a}{\mathrm{d}t} = \mu \left(\frac{a}{a_0}\right)^{-1/2} (1-e^2)^{-1} \left(\frac{D}{D_0}\right)^{-1} \cos\phi, \tag{10}$$

where the constant μ is

$$\mu = \dot{a}_0 \left(\frac{1-A}{1-A_0}\right)\left(\frac{\rho_0}{\rho}\right)\left(\frac{1-e_0^2}{\cos\phi_0}\right) \tag{11}$$

and $\dot{a}_0$ is the rate of variation of the semimajor axis for an object with semimajor axis a_0, eccentricity e_0, diameter D_0, density ρ_0, obliquity ϕ_0, and albedo A_0. We separate in equation (10) the contribution of the density and albedo because we suppose in our simulations that such quantities are the same for all members.

An estimation of the typical value for $\dot{a}_0$ could be deduced from the data in literature (Milani et al. 2014, table 10). In this work, we put $\dot{a}_0 \sim 3.3 \times 10^{-10}$ au yr^{-1}, for $a_0 = 1$ au, $e_0 = 0$, $D_0 = 1$ km, $\rho_0 = 2.4$ gr cm^{-3}, $\phi_0 = 0$, and $A_0 = 0$.

We assume that the value of the eccentricity of a single member does not change with time. We believe that this is a reasonable hypothesis from a statistical point of view. Assuming that no other parameter changes with time except the semimajor axis, if its value at the epoch t_1 is a_1, then the value at $t_2 > t_1$ is

$$a_2^{3/2} = a_1^{3/2} + \frac{3}{2}\xi(t_2 - t_1), \tag{12}$$

where

$$\xi = \mu a_0^{1/2}(1-e^2)^{-1}\left(\frac{D}{D_0}\right)^{-1}\cos\phi. \tag{13}$$

The Formula (12) is used to compute the variation of the semimajor axis during an interval of time $[t_1, t_2]$, during which the obliquity ϕ of the spin axis does not change.

The spin axes of asteroids in the Main Belt can change as a consequence of YORP effect and the non-destructive collisions with other projectile-asteroids, the impact energy of which is not enough to fragment and disperse the target-asteroid. YORP torque produces a modification of both spin direction and rotation period (Rubincam 2000; Čapek & Vokrouhlický 2004; Vokrouhlický et al. 2007). The most relevant feature of the YORP effect is the fast evolution of the obliquity angle towards the two equilibrium values: $\phi = 0$ for initial $\cos\phi > 0$ and $\phi = \pi$ if the initial $\cos\phi < 0$, hence without changing the direction of the semimajor axis drift (that is the sign of ξ in equation 12). The typical time-scale of this evolution is proportional to D^2, producing in principle differential effects among small bodies with respect to larger ones (Paolicchi & Knežević 2016). On the other hand, the real evolution of the rotational state of an asteroid due to the YORP effect depends dramatically on the details of the object's shape and surface (Statler 2009; Golubov & Krugly 2012; Ševeček et al. 2015; Marzari et al. 2020), and it would be more appropriate to talk about 'stochastic YORP' (Bottke et al. 2015; Cotto-Figueroa et al. 2015). We will devote a future paper to the investigation of the role of YORP effect on the determination of the age of the asteroid families.

For what regards the non-destructive collisions, their final effect, apart from the formation of craters and asteroid erosion, consist of a transfer of linear (Dell'Oro & Cellino 2007) and angular momentum (Harris 1979). The efficiency of the linear momentum transfer depends mainly on the poorly constrained sub-kilometre size distribution of the Main Belt asteroids. In order to avoid to introduce too many free parameters in our evolution model, we neglect this mechanism for the moment. Focusing on the collisional modification of the spins, their evolution is intrinsically stochastic. In our model, we assume that the characteristic time-scale τ_{rot} of the 'spin reset' due to collisions, consisting in a random modification of the rotational axis losing any memory of the previous state, can be expressed in general as

$$\tau_{\mathrm{rot}} = \tau_{\mathrm{rot},0}\left(\frac{D}{D_0}\right)^{\epsilon}, \tag{14}$$

where $\tau_{\mathrm{rot},0}$ and ϵ are free parameters. In this paper, we adopt the parameter values proposed by Farinella et al. (1998), that is, if $D_0 =$ 1 km, $\tau_{\mathrm{rot},0} = 7.5 \times 10^7$ yr. For what concerns the exponent, $\epsilon =$ 4/3 assuming a rotational period of 5 h for all objects, or $\epsilon = 1/2$ if the rotational period is proportional to D and $P = 5$ h for $D = 1$ km (Farinella et al. 1998; Brož & Morbidelli 2013). The two cases are plotted in Fig. 3.

On the basis of equations (12) and (14), in our model the post-formation evolution of the semimajor axis is numerically simulated by means of a Monte Carlo approach in the following way. Let us

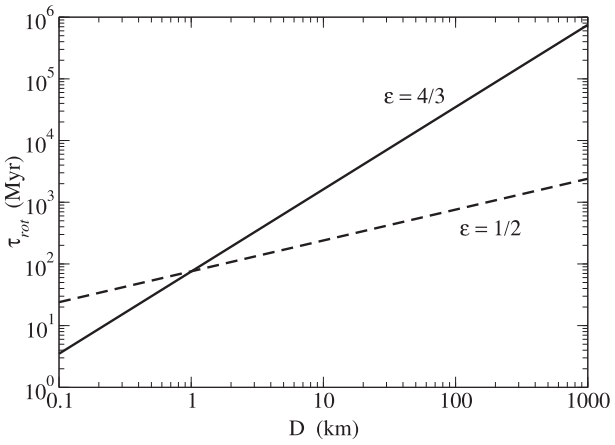

Figure 3. Characteristic time of rotational axis collisional re-orientation versus diameter for Main Belt Asteroids, according to the model by Farinella et al. (1998).

suppose that we want to simulate the evolution of the semimajor axis a of an asteroid with diameter D during the interval of time from $t = 0$ to $t = T$. During this interval of time, a number of collisional events producing a spin reset can occur at epochs $t_1, t_2, t_3, ..., t_n$, where $t_i < t_{i+1}$, and $t_1 > 0$, $t_n < T$. The number n of events is a random variate with a Poisson parent distribution with mean value $T/\tau_{\rm rot}$. In turn, the durations $\Delta t_i = t_{i+1} - t_i$ of each subinterval $[t_i, t_{i+1}]$ are random variates, all with the same probability distribution:

$$q(\Delta t) = \lambda e^{-\lambda \Delta t}, \tag{15}$$

that is the well-known waiting time distribution in a Poisson process, where $\lambda = 1/\tau_{\rm rot}$ is the mean number of events per unit of time.

Once the series of subintervals $[t_i, t_{i+1}]$ is generated, it is possible to compute the corresponding variations of the semimajor axis by means of equation (12), regenerating each time the spin vector **s**. From one subinterval to the next one, the new spin direction is randomly chosen, changing the obliquity value ϕ, and in turn the value of ξ in equation (12). It is worthwhile to note that in different subintervals the direction of the semimajor axis drift can be different, sometimes increasing ($\xi > 0$) and sometimes decreasing ($\xi < 0$). In conclusion, introducing the spin re-orientation, the evolution of the semimajor axis is no longer continuous and it becomes a random walk, where the final value is a stochastic quantity.

In our model, the evolution of the semimajor axis due to the Yarkovsky effect does not depend on the rotational period, or in other words on the magnitude s of the vector **s**. This is not completely correct but it is a simplification stemming from the use of the expression (10) for the mean typical rate of semimajor axis variation in the Main Belt.

3 ANALYSIS OF THE a-1/D DIAGRAM

The aim of this work is to investigate how some physical and dynamical mechanisms affect the determination of the age of an asteroid family. The observables of the asteroid family are simulated using the semi-analytical model discussed in the previous section. The determination of the age is based on the method proposed by Milani et al. (2014) and Spoto et al. (2015). The method details are widely described in the two quoted papers. Here, we shall summarize only the basic principles of the approach.

The input data necessary to estimate the age of an asteroid family are the list of the values of diameter and semimajor axis (D_k, a_k) for each member. The observational evidence that the large majority of the observed asteroid families show a negative correlation between the value of the diameter and the dispersion of the semimajor axes is interpreted as the result of the post-formation evolution due to the Yarkovsky effect. More in particular, the fact that in the diagram 1/D versus a the points representing the family members are constrained in a triangular or 'V-shaped' region, where the smaller members are more dispersed in semimajor axis than larger members, is considered to be a clear product of a semimajor axis drift proportional to 1/D, typical of the Yarkovsky effect (Cellino, Dell'Oro & Zappalà 2004). The objects close to the inner and outer border of the V-shape would be the fastest members of the family, those for which the absolute value of the rate of variation da/dt is maximum. In other words, the family borders are drawn by the members the obliquity of which is $\phi = 0$ (outer border) or $\phi = \pi$ (inner border). In conclusion, we expect that the borders of the V-shape are more or less linear, apart from deviations due to random fluctuations or the presence of family interlopers, and they can be determined by means of a linear fit of the points for which Δa, that is the difference between the semimajor axis of a member and of the parent body, is maximum or minimum (see Spoto et al. 2015 for details).

The result of this exercise is two lines in the diagram 1/D versus a, one for the inner border:

$$\frac{1}{D} = \frac{1}{u_-}(a - a_-) \tag{16}$$

and one for the outer border:

$$\frac{1}{D} = \frac{1}{u_+}(a - a_+), \tag{17}$$

where u_- and u_+ are the inverse slopes of lines fitting the inner and outer border, respectively, while a_- and a_+ are the positions where the two lines cross the horizontal axis (where $1/D = 0$). Hereinafter, the sign + refers to a quantity related to the outer border of the V-shape, while − refers to the inner border.

Following Milani et al. (2014), we call V-base the segment on the horizontal axis between the abscissas a_- and a_+ of the two fitting lines. The size of the V-base is the difference:

$$b = a_+ - a_-. \tag{18}$$

As we will see b is an interesting parameter. Here, we limit ourselves to say that if the two fitting lines cross above the horizontal axis the V-base size is negative, on the contrary if they cross under the horizontal axis the V-base size is positive. Finally, the middle point $(a_+ + a_-)/2$ is the centre of the V-base, and we will call relative centre of the V-base the quantity:

$$\delta = \frac{a_+ + a_-}{2} - a_{pb} \tag{19}$$

that is the difference between the V-base centre and the semimajor axis of the parent body.

The nature of the method requires that those family members with extreme values of the semimajor axis, inside interval bins of 1/D, are identified. From this point of view, the use of a Maxwell distribution for the generation of the ejection velocities, and therefore the initial semimajor axes, can produce some problems. The Maxwell one is not a domain-limited distribution, so that the above defined value of x_M has no upper limit. This means that, in a sequence of simulations with increasing number of family members, without changing all other model parameters, the probability of obtaining larger and larger values of Δa increases. Consequently, the values of the inverse slopes and the corresponding estimated ages tend to increase with the number of family members only. A way to

make more realistic our model for what regards the generation of the ejection velocity can be that suggested by Petit & Farinella (1993), consisting in putting as upper limit of the ejection velocities a value of the order of the sound speed in rock, that is about 3000 m s^{-1}. On the other hand, this approach does not solve the problem in our case because the analysis of real V-shape is limited to members not smaller than 1 km. Generating an ejection velocity of the order of the sound speed for $D = 1$ km requires very large and unrealistic values of v_0 and/or very large number of members (trials). For example, assuming $v_m = 1$ km s^{-1} at $D = 1$ km, at least 20 000 members of that size have to be generated to have the chance of obtaining at least one body with $v_{ej} \sim 3$ km s^{-1}. Taking into account that only the transverse component of the ejection velocity is relevant, the probability is even much smaller. For this reason we avoided to use Maxwellian ejection velocities in the numerical experiments discussed in this work, putting $m_v = 0$ in all cases.

At this point, two fundamental assumptions are introduced in the method of determination of the age of the family proposed by Milani et al. (2014). First, the V-shape is the result of the Yarkovsky effect alone, in the sense that the contribution of the initial ejection velocity field is negligible. In other words, the initial dispersion of the differences Δa for all the members of the family was much smaller than the present dispersion, that is in the diagram $1/D$ versus a the initial positions of the dots representing the family members coincide with the position of the parent body. Second, the semimajor axis drift rates due to the Yarkovsky effect are constant in value and direction, that is the difference Δa for each member is proportional to time. If those two assumptions are true, the inverse slopes of the border contain direct information about the age of the family, and more precisely, the inverse slopes are proportional to the family age. Therefore, the estimated age of the family would be:

$$T_{\mathrm{est}\pm} = \frac{|u_\pm|}{C}, \tag{20}$$

where C is a 'calibration' constant obtained from independent evaluation of the Yarkovsky effect. For this purpose, Milani et al. (2014) and Spoto et al. (2015) used a value of the calibration constant derived by the analysis of the orbital perturbations of the asteroid (101955) Bennu.

The scheme described above is obviously idealized. In the following sections, we will discuss some of the hypotheses this method of age estimation relies on. However, even from the observational point of view, the situation looks more complex. Apart from the problem that in some cases the V-shape borders are more or less polluted by interlopers that deteriorate the quality of the fit, among real families is not uncommon to come across case for which $|u_-| \neq u_+$, with the consequence that two solutions for the estimated age exist for a single family, and/or $b \neq 0$. This can be due to different causes, as discussed in Spoto et al. (2015) and Milani et al. (2019). In any case, in all our simulations the estimated age is always *formally* defined by equation (20), as opposed to the real age T_{real} the simulation is made for. From a different point of view, T_{real} is a physical parameter while $T_{\mathrm{est}\pm}$ is a geometrical property of the V-shape (as $u_\pm$ are) that can be interpreted as an estimator of T_{real} if some hypotheses are met. In our simulations, the calibration constant C depends on the value of the parameter $\dot{a}_0$ in equation (11), along with the eccentricities, albedos, and densities of the members. We determine the value of C on the basis of a simulation that meets entirely the above mentioned hypotheses of the age estimation method. The parameters of such reference simulation are: fully isotropic spin–velocity field ($\eta_v = \eta_s = \pi$); ejection velocities negligible ($v_0 = 0$); collisional spin reset disabled ($\tau_{rot,0} = \infty$), entailing constant semimajor axes drift rates. The value of C is the constant ratio between the inverse slope u (in this case the isotropy of the ejection velocities entails that $|u_-| = u_+$) and the real age T_{real} the simulation refers to.

Although in our reference simulation, the spin–velocity field is perfectly symmetric, $|u_-|$ does not turn out to be exactly equal to u_+, and moreover the ratios $u_\pm/T_{\mathrm{real}}$ are not strictly constant. Apart from random fluctuations due to the process of generation of the velocity field, $|u_-|$ tends to be systematically larger than u_+, and the difference increases with time. This is simply due to the semimajor axis evolution predicted by equation (12), since the semimajor axis drift rate (according to equation 10) depends on the semimajor axis itself as $a^{-1/2}$. This means that the Yarkovsky drift rate tends to increase for an object the semimajor axis of which is decreasing, while it tends to decrease for an object the semimajor axis of which is increasing. This Yarkovsky acceleration/deceleration produces an accelerated expansion of the inner part of the V-shape and a decelerated expansion of the outer part, as shown in Fig. 4, top right. The result, even in the reference simulation, is that for larger and larger values of T_{real} absolute value of the inner inverse slope $|u_-|$ tends to increase faster than the outer inverse slope u_+ and, in turn, the ratio $|u_-|/T_{\mathrm{real}}$ tends to increase with T_{real}, while u_+/T_{real} tends to decrease with T_{real}. In order to make the definition of T_{est} formally consistent we define C as the ratio $u_\pm/T_{\mathrm{real}}$ for $T_{\mathrm{real}} \to 0$, where $u_\pm$ is the inverse slopes of the reference simulation. This affects the values $T_{\mathrm{est}\pm}$ of this simulation, with $T_{\mathrm{est}-}$ increasing more than T_{real} and $T_{\mathrm{est}+}$ increasing less than T_{real} (Fig. 4, bottom left).

Even if this acceleration/deceleration physical process is realistic, the distortion of the V-shape produced by this mechanism requires large values of T_{real}, and we do not expect that it can produce relevant observational effects for the majority of the real asteroid families, probably negligible with respect to the other effects that we will discuss later. Attempts to detect a systematic difference between $|u_-|$ and u_+ among real asteroid families have not been successful until now.

The Yarkovsky acceleration/deceleration produces effects also on the V-base, both for what concerns its size and the centre. At the beginning of the asteroid family evolution, for $T_{\mathrm{real}} = 0$, the initial values of b and δ are null. At a time $T_{\mathrm{real}} > 0$, the geometrical distortion of the V-shape makes b negative (the fitting lines cross above the horizontal axis) and δ positive (Fig. 4, bottom right). As time passes b becomes more and more negative, while δ becomes more and more positive.

The plots in Fig. 4 describe the results of a particular reference simulation. An important feature of all the parameters of the border fit (and their related quantities like the estimated age $T_{\mathrm{est}\pm}$) is that they are not deterministic values but rather random variables. Both in our simulation, and in real asteroid families, the disposition of the members on the V-shape borders is, with some limits, a random process because of the family formation mechanism and the subsequent evolution. For the real asteroid families we do not know the details of the primordial break-up, both for our approximate knowledge of the fragmentation and dispersion mechanism and for the intrinsic stochastic nature of the collision event producing the break-up. In our model, this is due to the random nature of the generation of the list of member diameters, their velocities, and spins. Moreover, if spin-reset mechanisms are at work during the evolution of the family, other fluctuations are introduced. All other parameters of the model fixed, the extent of fluctuations and in some cases the shapes of their statistical distributions depend on the number of members the asteroid family consists of. For these reasons, it is important to check the resulting distribution of the fitting parameters as the result of an adequate number of repeated

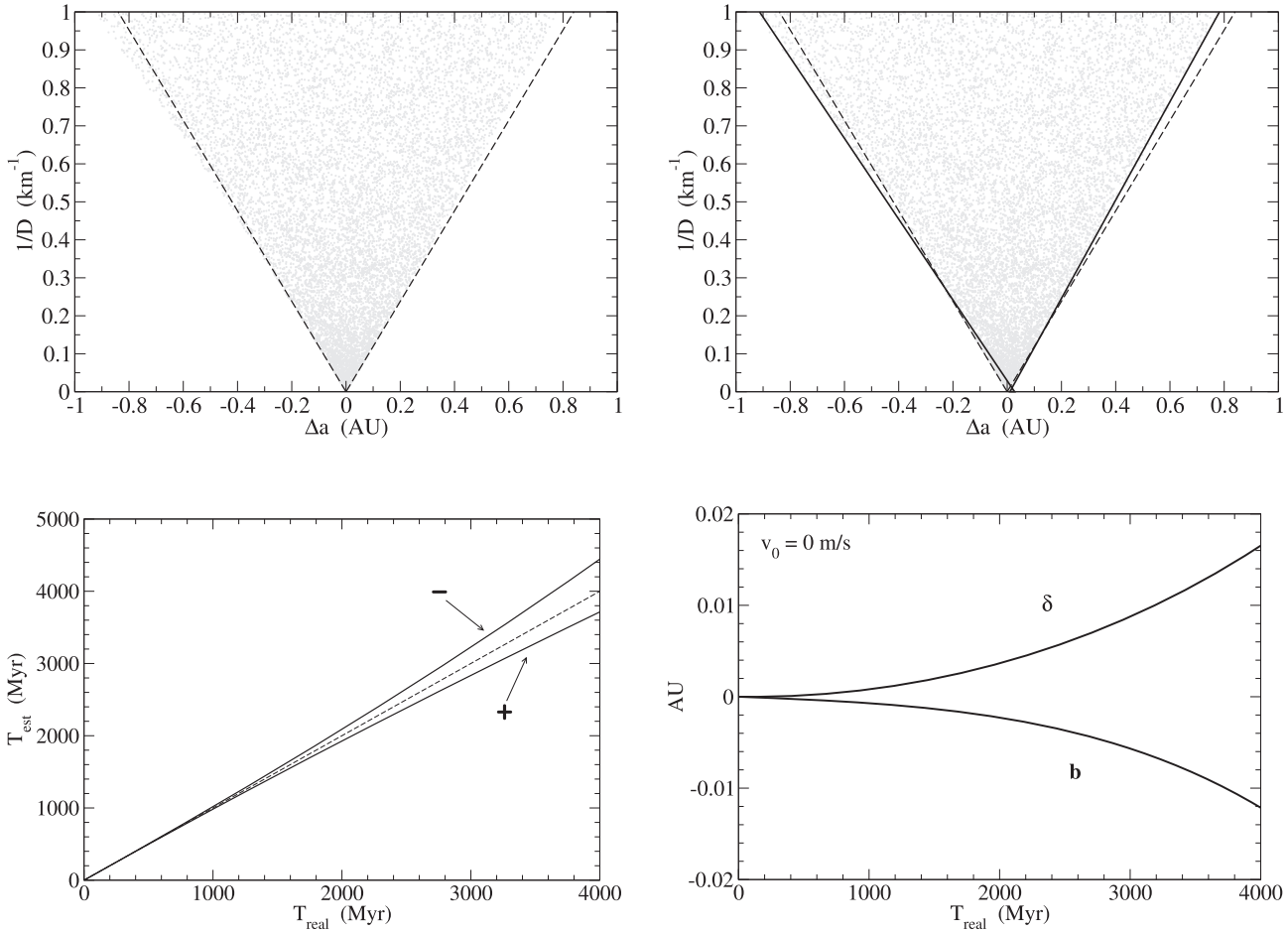

Figure 4. Top: Deformation of the V-shape borders due to the acceleration/deceleration of the Yarkovsky drift rate in our reference simulation. $T_{\rm real} = 4$ Gyr in order to make the effect more visible. The two dashed lines represent the expected borders of the V-shape if the semimajor axis drift rate had been strictly constant, while the solid lines represents the best-fitting lines of the V-shape borders. Bottom left: Behaviour of the estimated ages $T_{\rm est\pm}$ versus $T_{\rm real}$ computed according to the definition explained in the text, for the reference simulation. Bottom right: V-base size b and relative centre of the V-base δ versus real age $T_{\rm real}$, for the reference simulation.

simulations, not relying on the result of a single simulation only. Fig. 5 shows the statistical distributions of the estimation age biases and the geometrical parameters b and δ, and their evolution at different time-steps. In particular, the distributions of b and δ tend to be particularly wide. This is a point that will be discussed later in the context of the role of the gravitational reaccumulation.

4 INFLUENCE OF PHYSICAL EFFECTS

In the following sections, we will show and discuss the results of some numerical simulations. In all simulations, the orbital elements of the parent body are $a_{pb} = 2.55$ au, $e_{pb} = 0.1$, and $I_{pb} = 10$ deg, while its true anomaly at the epoch of the break-up is $f_{pb} = 90$ deg. In all cases, the velocity part of the spin–velocity field is isotropic, that is $\eta_v = \pi$.

The choice of a_{pb}, e_{pb}, and I_{pb} corresponds to a typical location in the Main Belt Asteroids. Different values of those orbital elements modify the details of the simulation outcomes leaving the main conclusions unchanged. For what regards the choice of f_{pb}, in addition to the fact that $f_{pb} = 90$ and 270 deg are more or less the most probable values at the moment of the impact (Dell'Oro & Paolicchi 1998), the value of f_{pb} affects only marginally the distribution of the semimajor axes of the asteroid family (Zappalà et al. 1996).

By choosing the parameters above, the value of the calibration constant C, determined as described in Section 3, turns out to be equal to 2.1×10^{-10} au km yr^{-1}.

The aim of the numerical simulations is to enlighten the impact of different physical mechanisms that can modify the structure of the V-shapes introducing a bias in the determination of the asteroid family ages. Such bias can be expressed in terms of the difference between the estimated age and the real age:

$$\Delta T_{\pm} = T_{\rm est\pm} - T_{\rm real}. \quad (21)$$

Besides studying how the bias $\Delta T_{\pm}$ depends on the physical parameters of the model, it is interesting to investigate how it varies with $T_{\rm real}$. Indeed $T_{\rm est\pm}$ is a complex function of $T_{\rm real}$, the trend of which depends on the assumptions about the formation and evolution of the asteroid family. In the following, we will examine the effect of each single assumption separately.

4.1 The initial velocity field

In general, for real asteroid families, we cannot expect that $\Delta T_{\pm} = 0$ if $T_{\rm real} = 0$. The reason is that the break-up velocity field introduces an initial non-null spreading of the orbital elements, depending directly on the value of the exit velocities. Any fit of the V-shape borders of

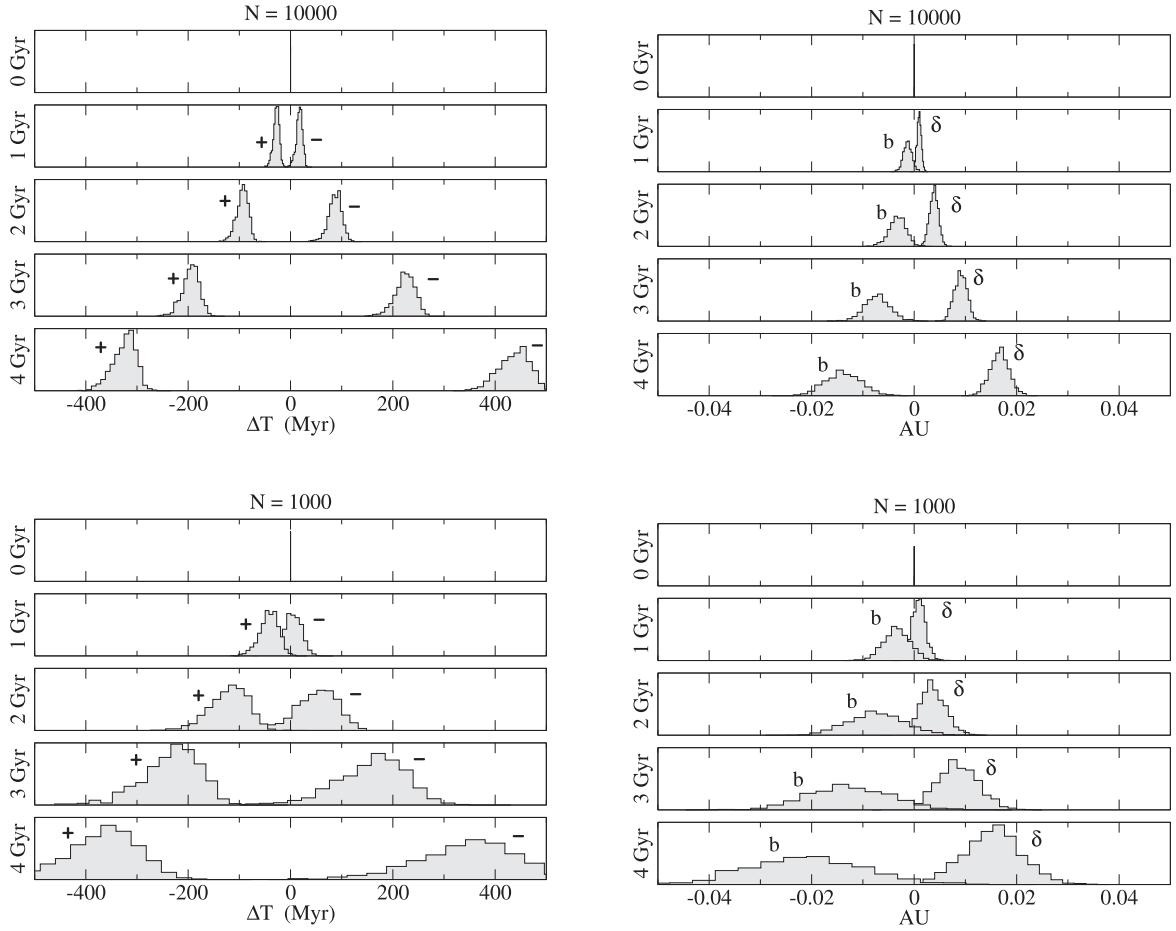

Figure 5. Reference simulation: Statistical distributions of the age estimation bias $\Delta T_{\pm} = T_{\mathrm{est}\,\pm} - T_{\mathrm{real}}$ (left), and statistical distributions of the V-base size b and of the relative centre δ of the V-base (right). The two cases of 10 000 members (top) and 1000 members (bottom) are displayed.

a family at $T_{\mathrm{real}} = 0$ will produce necessarily a value of $T_{\mathrm{est}\,\pm} > 0$, and so a positive bias $\Delta T_{\pm}$. The magnitude of this initial bias can be quantified simulating asteroid families with different values of v_0. Since the initial orbital spreading depends on the distribution of the exit velocities we put here the parameter $D_{\mathrm{lim}} = \infty$ in order to exclude the effect of the gravitational reaccumulation. In this way, ejection and exit velocities coincide and v_0 is the maximum value of the exit velocity for fragments one kilometre in size.

Fitting the borders of the V-shape of a series of asteroid families, all at $T_{\mathrm{real}} = 0$ but characterized by different values of v_0, we obtain values of $T_{\mathrm{est}\,\pm}$ more or less proportional to v_0 as shown in Fig. 6. This is obviously not an unexpected result, which can be easily derived from the Gauss' formulas in the assumption that $\beta = 1$. Indeed the inverse slope results to be $|u_{\pm}| = (2/n)D_0 v_0$ (see Appendix B for details), which implies an initial estimated age (and bias) $\Delta T_{\pm}(0) = T_{\mathrm{est}\,\pm}(0) \sim 1.3$ Myr if $v_0 = 1$ m s^{-1} (recalling that by definition $D_0 = 1$ km).

But, once again in the numerical simulations, a small difference between $T_{\mathrm{est}\,-}$ and $T_{\mathrm{est}\,+}$ arises. The difference comes from the fact that the transformation from the exit velocities to the initial orbital elements is not linear. Gauss' equations are correct only at the first order with respect to the velocities. An isotropic ejection velocities distribution does not correspond to a distribution of the semimajor axes exactly symmetric with respect to the value of the semimajor axis of the parent body. In particular, the extension in terms of a of the family for $a > a_{pb}$ is larger than for $a < a_{pb}$. This explains why the initial V-shape outer border appears more 'evolved' with respect to the inner border. In any case the effect is small, amounting to a difference of about 10 Myr between $T_{\mathrm{est}\,+}$ and $T_{\mathrm{est}\,-}$ for $v_0 = 100$ m s^{-1}.

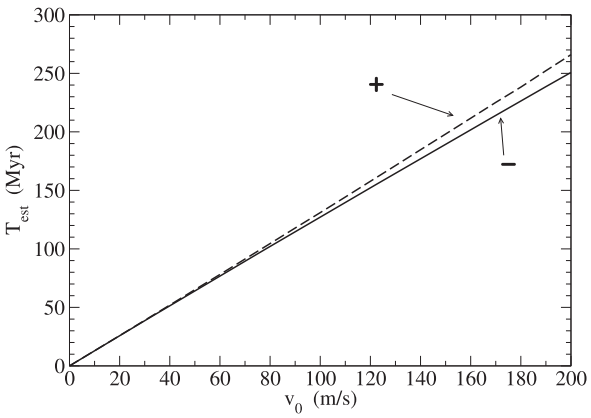

Figure 6. Estimated ages (solid line: $T_{\mathrm{est}\,-}$; dashed line: $T_{\mathrm{est}\,+}$) versus v_0, for a not yet evolved asteroid family ($T_{\mathrm{real}} = 0$), characterized by a non-null velocity field.

Let us move on to discuss what happens during the evolution of an asteroid family with non-null initial velocity field. Fig. 7 shows the case of an asteroid family with $v_0 = 100$ m s^{-1}, the evolution of

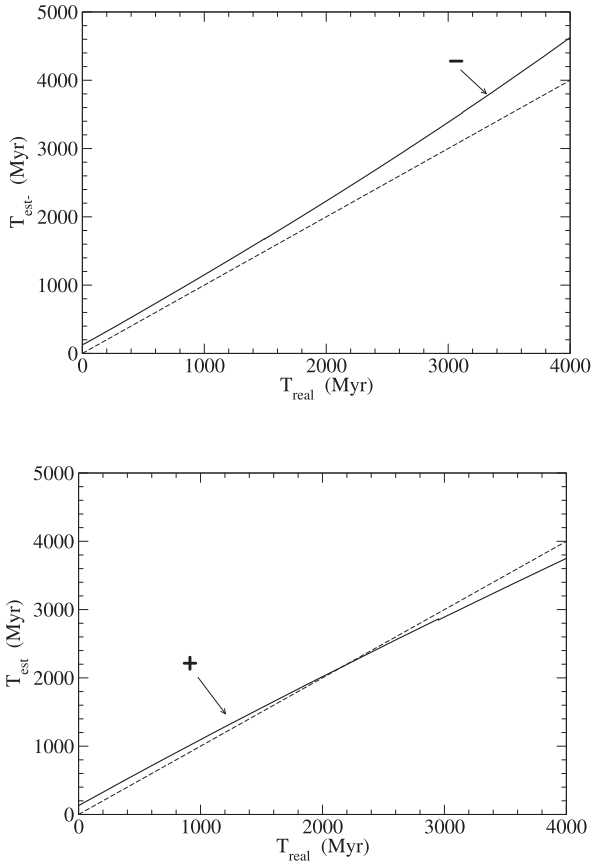

Figure 7. Evolution of an isotropic family with $v_0 = 100$ m s^{-1}. Top: $T_{\mathrm{est}-}$ versus T_{real}. Bottom: $T_{\mathrm{est}+}$ versus T_{real}. The dashed line represents function $T_{\mathrm{est}\pm} = T_{\mathrm{real}}$.

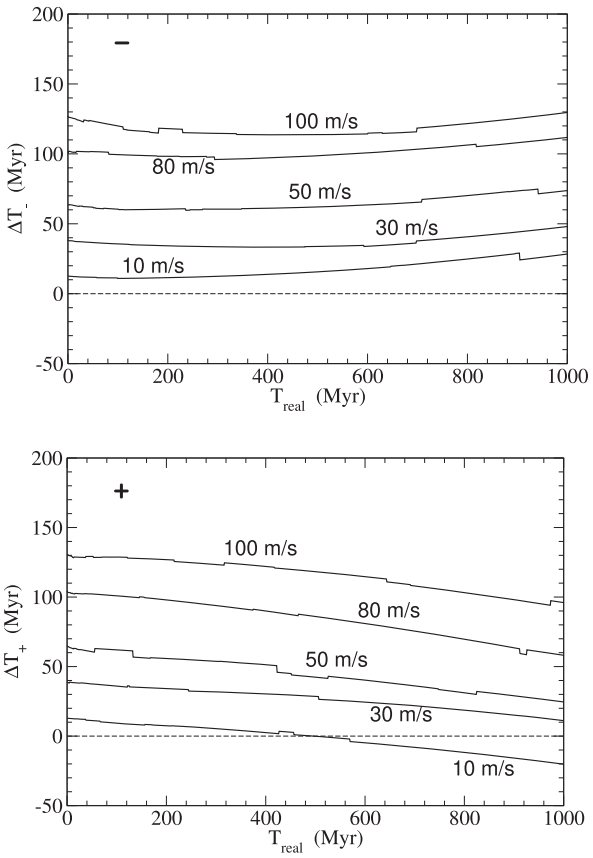

Figure 8. Top: Bias of estimated age versus real age for isotropic families with different values of v_0 obtained from the inverse slope of the V-shape inner border. Bottom: The same but obtained from the outer border.

which is followed up to 4 Gyr. Apart from the initial small difference between $T_{\mathrm{est}+}$ and $T_{\mathrm{est}-}$ due to the above mentioned asymmetry of the initial orbital distribution, it is noticeable again the effect of the Yarkovsky acceleration on $T_{\mathrm{est}-}$ (left) and of the Yarkovsky deceleration on $T_{\mathrm{est}+}$ (right). While the initial bias on $T_{\mathrm{est}-}$ will never be overridden, but rather it is amplified, the initial bias on $T_{\mathrm{est}+}$ is cancelled out after about 2 Gyr and subsequently overcorrected. Those trends are clearly shown in Fig. 8 where the biases $\Delta T_{\pm}$ are plotted versus T_{real} between $T_{\mathrm{real}} = 0$ Gyr and $T_{\mathrm{real}} = 1$ Gyr, for different values of v_0. The bias ΔT_- tends to decrease slightly to a minimum value (that in the case of $v_0 = 100$ m s^{-1} is at about 500 Myr), and then to rise steadily. The bias ΔT_+, initially positive, steadily decreases first becoming null and then negative. The epoch T_{real} when $\Delta T_+ = 0$ increases with v_0.

The jumps in the curve plotted in Fig. 8 are due to the random statistical fluctuations in the generation of the ejection velocities. It can happen that, during the V-shape expansion, some fast members initially placed in the core of the family overtake the members on the border affecting the determination of the inverse slope.

4.2 Velocity–spin correlation

As discussed in Section 2.1, our model allows different degrees of correlation between the ejection velocity and the rotational spin of a fragment. The existence, in a catastrophic disruption, of a relationship between the rotational properties of a fragment and the place in the parent body where it was ejected from has been discussed in several works in literature (Fujiwara & Tsukamoto 1981; Fujiwara et al. 1989; Giblin et al. 1994; Holsapple et al. 2002; Kadono et al. 2009). From a theoretical point of view, the experimental evidence concerning the distribution of the ejection velocities has been analytically implemented in the semi-empirical model by Paolicchi et al. (1989) and Paolicchi, Verlicchi & Cellino (1996). In this model, a collision event involving a parent body is described in terms of the velocity field $\boldsymbol{v}(P)$, assigning an initial velocity $\boldsymbol{v}$ to any point P inside the body. The analytical properties of the velocity field, along with some plausible physical assumptions about the material reaction to impact stress, determine shapes, dimensions, ejection velocities, and rotational properties of the fragments. In particular, the spin axis is parallel to the curl $\nabla \times \boldsymbol{v}$ of the velocity field. For a non-rotating target, the velocity field is radial with respect to an irradiation point inside the body and cylindrically symmetric around an axis parallel to the impact direction and containing the irradiation point. In this hypothesis, the curl of the velocity field is normal to both the velocity and the symmetry axis $\hat{\boldsymbol{k}}$. In terms of the parameters of our model, this situation corresponds to $\hat{\boldsymbol{h}} = \hat{\boldsymbol{p}}$ ($\theta_h = 0$) and $\eta_s = 0$ (or simply $\mathbf{s}$ is parallel to $\hat{\boldsymbol{p}}$, see Fig. 1).

This configuration can give rise to more or less strong correlations between the components of the ejection velocity and the components of the spin axis, and in particular with the transverse component v_T of the ejection velocity (see Appendix A for details). At the zero-order of the Gauss' equations, the initial difference between the semimajor axis of the fragment and the semimajor axis of the parent body is $\Delta a = (2/n)v_T$, with n the parent body's mean orbital motion. So, any correlation between v_T and s_N (the component of the spin axis along

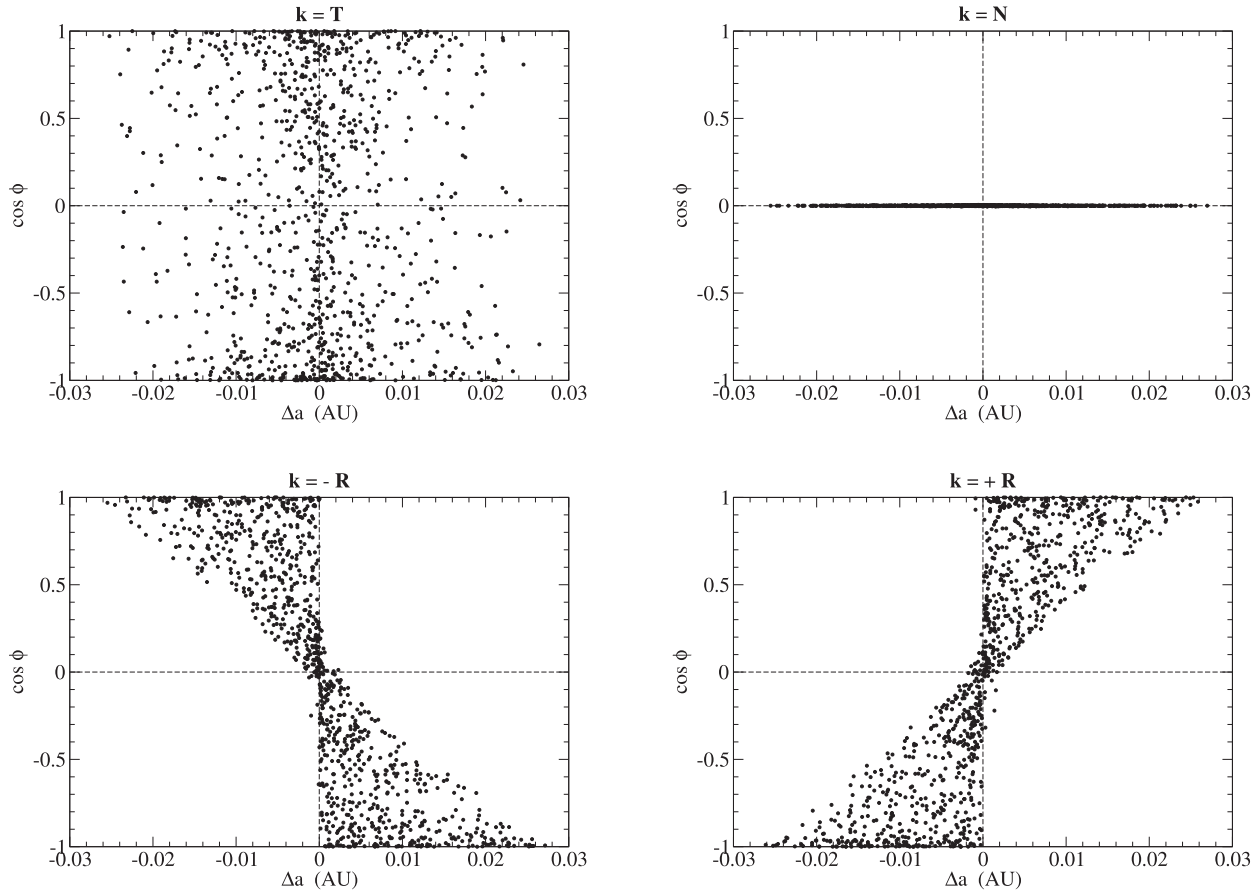

Figure 9. Spin–velocity field with $\theta_h = 0$ and $\eta_s = 0$. The plots show the $\cos\phi$ versus Δa for different directions of the symmetry axis $\hat{\boldsymbol{k}}$: $\hat{\boldsymbol{k}} = \pm\boldsymbol{T}$ (top left), $\hat{\boldsymbol{k}} = \pm\boldsymbol{N}$ (top right), $\hat{\boldsymbol{k}} = -\boldsymbol{R}$ (bottom left), and $\hat{\boldsymbol{k}} = +\boldsymbol{R}$ (bottom right).

the normal to the orbit) produces a correlation between the initial position of the fragment in the V-shape diagram and the direction of the Yarkovsky drift, depending on the cosine of the obliquity $\cos\phi = s_N/s$.

Once $\theta_h = 0$ and $\eta_s = 0$, the correlation between $\cos\phi$ and Δa depends on the orientation of the symmetry axis $\hat{\boldsymbol{k}}$. Three extreme configurations are possible. If $\hat{\boldsymbol{k}} = \pm\hat{\boldsymbol{T}}$, that is $\theta_k = \pi/2$ and $\lambda_k = \pi/2$, $3\pi/2$, no correlation $\cos\phi$–Δa exists, as shown in Fig. 9 at top left. This situation is similar to what happens when a complete randomization of the spin–velocity field is set ($\eta_s = \pi$). If $\hat{\boldsymbol{k}} = \pm\hat{\boldsymbol{N}}$ ($\theta_k = 0$), the normal component of the spin axis is trivially null (Fig. 9, top right). In this case, not only $\cos\phi$ is not correlated with Δa, but also there is no Yarkovsky drift, if no other external perturbation is present.

The most interesting situation occurs when the symmetry axis is parallel to the radial direction. If $\hat{\boldsymbol{k}} = +\hat{\boldsymbol{R}}$, that is $\theta_k = \pi/2$ and $\lambda_k = 0$, a positive correlation exists between $\cos\phi$ and Δa (Fig. 9, bottom right). This means that all the family members initially placed at the right of the parent body in the $1/D$ versus a diagram increase with time their semimajor axis, and opposite for the members initially placed at the left of the parent body, producing an overall regular expansion of the V-shape. Instead if $\hat{\boldsymbol{k}} = -\hat{\boldsymbol{R}}$ ($\theta_k = \pi/2$ and $\lambda_k = \pi$), $\cos\phi$ and Δa are negatively correlated. In this case, all the family members initially placed at the right of the parent body in the $1/D$ versus a diagram decrease their semimajor axes, while all members initially placed at the left increase their semimajor axis. The consequence is an overall initial collapse of the V-shape, followed by an expansion after the semimajor axes of the members with initial negative Δa become larger than the parent body semimajor axis, and *vice versa*.

The correlations between $\cos\phi$ and Δa shown above have effects on the value of the estimated age of the family. While for $\hat{\boldsymbol{k}} = \pm\hat{\boldsymbol{N}}$ the evolution of the V-shape is prevented, or strongly restrained, until an external perturbation intervenes, for $\hat{\boldsymbol{k}} = \pm\hat{\boldsymbol{R}}$ the bias due to the initial dispersion of the semimajor axes is reinforced or removed. Fig. 10 shows the case of a family with $v_0 = 100$ m s^{-1} but the qualitative behaviour is the same for all values of v_0. The value of the bias $\Delta T_\pm$ versus $T_{\rm real}$ for a fully isotropic spin–velocity field is plotted as a grey line ($\eta_s = \pi$). In case of a positive correlation due to the condition $\hat{\boldsymbol{k}} = +\hat{\boldsymbol{R}}$, the bias $\Delta T_\pm$ is systematically larger than the bias introduced by the fully isotropic case. In other words, the distribution of the obliquities in the V-shape gives a faster V-shape expansion with respect to a random disposition. In the case $\hat{\boldsymbol{k}} = -\hat{\boldsymbol{R}}$, the initial collapse of the V-shape cancels out the bias introduced by the velocity field, resetting the evolution of the V-shape. The time required to 'absorb' the initial bias due to the velocity field depends on v_0 and is more or less equal to the initial bias itself (see Fig. 6). In other words in case $\hat{\boldsymbol{k}} = -\hat{\boldsymbol{R}}$ the situation is very close to what happens for an asteroid family with a negligible velocity field. Again the effect of the Yarkovsky acceleration/deceleration is evident. Apart from the usual jumps due to the random noise at the borders during the post-formation evolution of the family, the relative disposition of the three curves is systematic.

The initial velocity field could, for very young families, be responsible for the discrepancy between the age obtained by means

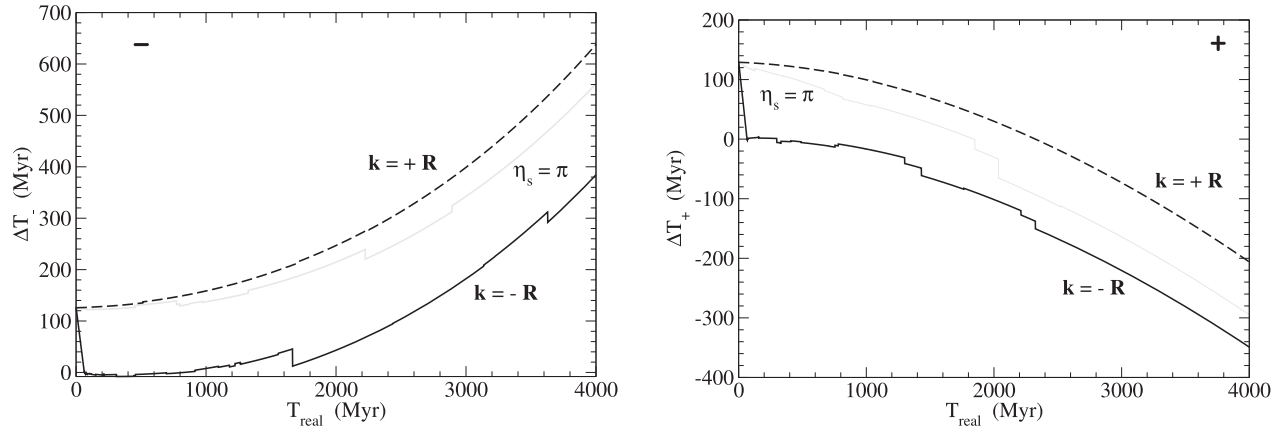

Figure 10. Evolution of the bias $\Delta T_{\pm}$ for a fully isotropic family (null correlation, grey line), a spin-polarized family with $\hat{\boldsymbol{k}} = +\hat{\boldsymbol{R}}$ (positive correlation, dashed line), and a spin-polarized family with $\hat{\boldsymbol{k}} = -\hat{\boldsymbol{R}}$ (negative correlation, solid line).

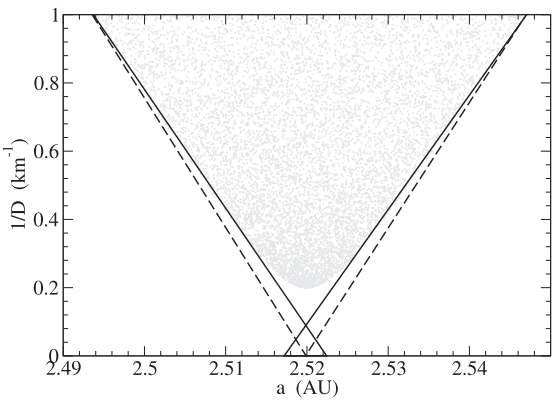

Figure 11. Deformation of the V-shape due to the effect of the gravitational reaccumulation. Dashed lines represent the V-shape borders in case of no reaccumulation. Solid lines represent the linear fit of the borders. The parameters of this case are: $v_0 = 100$ m s^{-1}, $D_{\rm lim} = 5$ km, and $T_{\rm real} = 0$.

of backward integration method and the one based on the analysis of the V-shape. In particular, a velocity–spin correlation can increase or reduce such discrepancy depending on the impact direction. A typical example is the family of (1547) Nele for which backward integration suggests that the family is younger than 7 Myr (Carruba et al. 2018), while V-shape fitting provides an age about 15 Myr (Spoto et al. 2015). In this respect, a larger V-shape-derived age should be compatible with a $\hat{\boldsymbol{k}} = +\hat{\boldsymbol{R}}$ -type collision. Such hypothesis deserves further investigation in future works.

4.3 Gravitational reaccumulation

Another physical mechanism influencing the structure of the V-shape is the gravitational reaccumulation during the primordial break-up process. As analytically discussed in Appendix B, values of the effective escape velocity $v_{\rm esc} \neq 0$ in equation (3) entail a modification of the borders of the V-shape in the part of small values of $1/D$. More exactly, in the cases taken into account in this work with $\beta = 1$ (see equation 2), the border of the V-shape becomes a hyperbola with asymptotes that correspond to the expected borders if no reaccumulation occurred ($v_{\rm esc} = 0$), as shown in Fig. 11. The ordinate of the vertex corresponds to the limiting value of the diameter $D_{\rm lim}$ given by equation (4). As a consequence, the two fitting lines do not

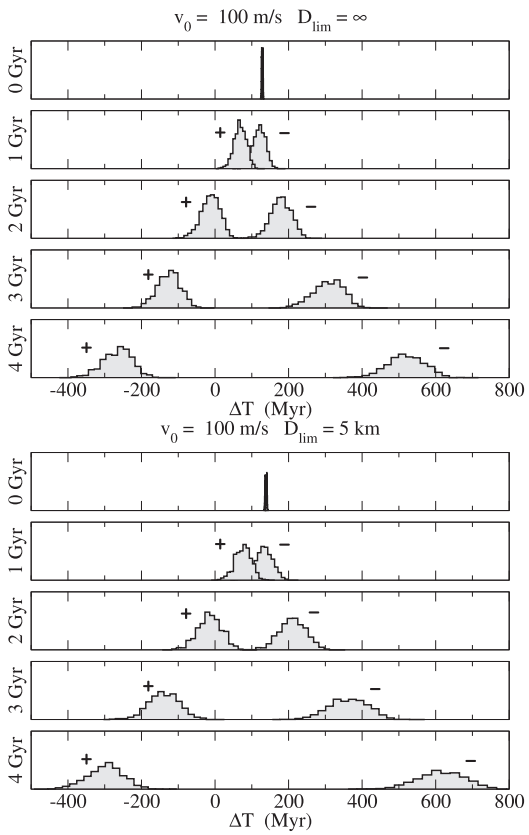

Figure 12. Statistical distributions of the estimated age bias, at different epochs $T_{\rm real}$, for a case with $v_0 = 100$ km s^{-1} without gravitational reaccumulation (top) and with reaccumulation (bottom).

coincide with the asymptotes but on one hand, their inverse slopes increase, increasing the estimated ages, and on the other, they cross above the horizontal axis $1/D = 0$ making the V-base negative.

The impact on the estimated ages is limited as shown in Fig. 12. For comparison, on the left a case of an asteroid family with $v_0 = 100$ m s^{-1} where no reaccumulation occurred ($D_{\rm lim} = \infty$) is shown. Looking at the averages of the statistical distributions we find again the same behaviour shown previously in Fig. 7. On the right, the same case is represented but with a reaccumulation producing a limiting

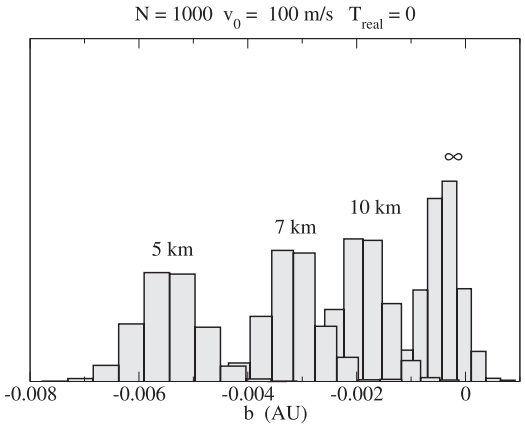

Figure 13. Distributions of the V-base b at $T_{\rm real} = 0$ for 1000 asteroid families with $v_0 = 100$ m s^{-1} consisting of 1000 members each. The numbers on top of each histogram are the corresponding values of the limit diameter $D_{\rm lim}$.

diameter $D_{\rm lim} = 5$ km. A very moderate increase (absolute value) of the age estimation biases occurs.

For what concerns the V-base size, its value b is directly affected by the degree of reaccumulation. Fig. 13 shows the initial statistical distributions of b at the epoch $T_{\rm real} = 0$ for the same family with $v_0 = 100$ m s^{-1} for different values of $D_{\rm lim}$. The smaller the limit diameter $D_{\rm lim}$ the more negative the mean value of b, while the variance decreases with increasing number of family members. During the subsequent evolution, the V-base and its dispersion increase as time passes. Fig. 14 shows how the statistical distribution of b evolves for the case of two families with $v_0 = 1$ m s^{-1} and $v_0 = 100$ m s^{-1}, with and without gravitational reaccumulation. Even if the temporal evolution is responsible for much of the final values of b, the reaccumulation reinforces this trend, especially by increasing the range of the possible (negative) values of b.

4.4 Collisional spin reset

The last physical mechanism capable of altering the V-shape structure of an asteroid family investigated in this work is the re-orientation of the rotation axes of the members due to non-destructive collisions with other asteroids. Unlike the processes discussed in the previous sections, the spin reset acts during the post-formation evolution of the family. The fundamental hypothesis underlying the method of determination of the asteroid families age based on the measure of the inverse slope of the V-shape border is that the direction and drift rate of the semimajor axis evolution are constant. We have seen in Section 3 that a non-negligible violation of the assumption of drift rate constancy is introduced by the intrinsic acceleration/deceleration of the Yarkovsky effect, as expected by equation (10). A much larger effect is due to the random re-orientation of the spin axis described in Section 2.3. Frequent inversions of the obliquity sign cause repeated inversions of the direction of variation of the semimajor axis. If the characteristic time of the spin reset is much smaller than the evolution interval of time, the motion of a point in the (a, 1/D) diagram is like a random walk parallel to the horizontal axis, consisting in a series of increases and decreases of the semimajor axis. In these conditions, the inverse slopes of the V-shape borders are no longer proportional to the family age but, more or less, to the root square of the family age. In fact, this is what results from the numerical simulation shown in Fig. 15 suggest. The growth of the inverse slope slows down steadily so that the gap between the real age and the estimated ages increases accordingly. The perturbed trends of the curves are due to the random fluctuations of the positions of the family members determining the V-shape borders.

The small difference between the case $\epsilon = 1/2$ and $\epsilon = 4/3$ is due to the fact that the two models of spin reset affect in different way the lower and upper regions of the V-shape. The case $\epsilon = 1/2$ is more homogeneous with respect to $\epsilon = 4/3$ in the sense that the difference in spin reset frequency between smaller and larger members is more restrained. The characteristic time $\tau_{\rm rot}$ is about 80 Myr at $D = 1$ km in both cases, while at $D = 100$ km $\tau_{\rm rot} \sim 800$ Myr for $\epsilon = 1/2$ and $\tau_{\rm rot} \sim 40$ Gyr for $\epsilon = 4/3$ (Fig. 3). The gradient of $\tau_{\rm rot}$ from small to large diameter produces a bending of the V-shape borders which is more pronounced for $\epsilon = 4/3$. In other terms, the diagram (a, 1/D) of the family is no longer a V-shape but rather a U-shape (Fig. 16). For $\epsilon = 4/3$, the evolution of the members with $D > 10$ km is practically unaffected by the spin reset. The curvature of the U-shape borders is more pronounced for $\epsilon = 4/3$ with the consequence that the inverse slope of the linear fit becomes smaller (and consequently the estimated age is smaller with respect to the case $\epsilon = 1/2$).

The bending of the V-shape borders has an even more noticeable effect on the value of the V-base b. If no spin reset existed, the evolution of the border points with a rate proportional to 1/D should not imply an intersection of the two fitting lines far away from the horizontal axis. But if the spin reset is at work, the bending of the V-shape border produces an intersection well below the horizontal axis 1/$D = 0$ (Fig. 16), or in other words a positive V-base. And the more time passes, the more the value of b increases, as shown in Fig. 17. The value of b is strongly affected by random fluctuations but the systematic trend is clear. The same figure at right shows the distribution of b for an ensemble of 1000 simulated asteroid families with 10 000 members each. The statistical fluctuations increase when the number of family members decreases but the evolution trend is the same.

Compared to the decrease of V-base size due to the gravitational reaccumulation, the increase of b caused by the spin reset dominates. Gravitational reaccumulation is responsible for values of b that cannot be less than -0.05 au, for velocity fields with v_0 of the order of 100 m s^{-1} at most, and taking into account evolution times up to 4 Gyr. After only 1 Gyr spin reset increases the V-base size by 0.05 au if $\epsilon = 4/3$, and about 0.025 au if $\epsilon = 1/2$, as it can be seen in Fig. 18 where the combined effect of reaccumulation and spin reset is shown.

5 CONCLUSIONS

In this paper, we have shown the results of a preliminary investigation of some physical processes affecting the analysis of the asteroid family V-shapes, mainly in order to estimate the time elapsed since their formation. We have discussed how each single process affects the geometrical properties of the V-shape and how much it impacts the determination of an asteroid family age. In order to carry out this investigation, we developed a numerical model of the family formation and evolution as flexible as possible in order to highlight the role of the different mechanisms.

The determination of the asteroid family ages by measuring the inverse slopes of their V-shape borders relies on the assumption that contribution of the initial ejection velocities of the family members is negligible. As expected, such assumption is particularly critical for very young families. We found that the initial off-set in millions of years in the age determination introduced by the break-up velocity field is of the order of typical exit velocities of the km-sized fragments expressed in metres per second. As explained

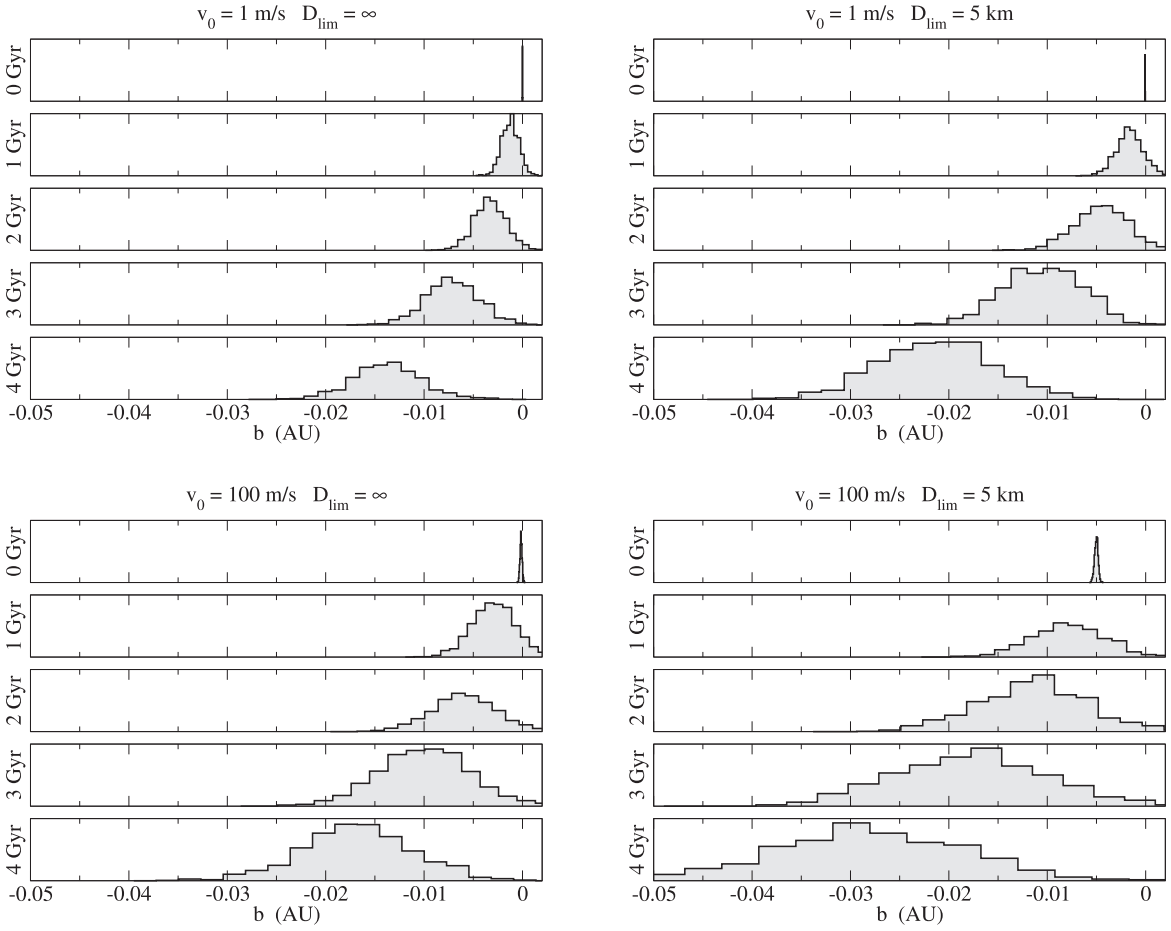

Figure 14. Evolution with time of the statistical distribution of the size of the V-base. Two different sizes of the ejection velocity field are taken into account ($v_0 = 1$ m s^{-1} at the top, and $v_0 = 100$ m s^{-1} at the bottom). Left: Evolution without initial gravitational reaccumulation. Right: Case with reacumulation with limit diameter $D_{\rm lim} = 5$ km. The number of family members is 10 000.

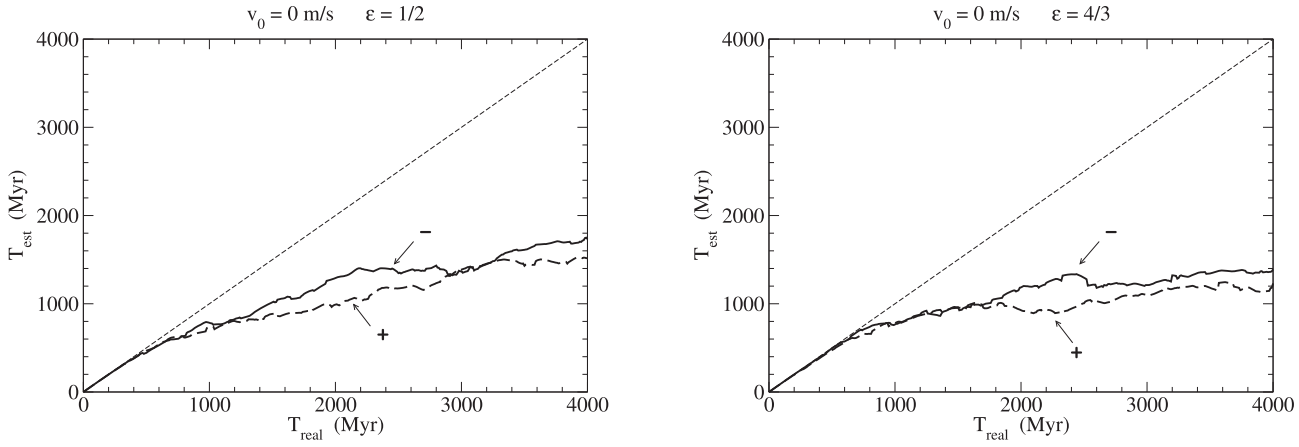

Figure 15. Estimated age versus real age of an asteroid family with $v_0 = 0$, when the collisional spin reset is active (left for $\epsilon = 1/2$, right for $\epsilon = 4/3$).

in Section 3, for technical reasons we avoided to use Maxwellian distribution of the ejection velocities, a choice that would have been more realistic but that would have introduced artificial effects into the results. As a consequence, the above estimation of the initial age bias should be considered as a lower limit. On the other hand, under the assumption that the post-formation evolution of the V-shape borders is determined by the Yarkovsky drift rate only, such initial bias is not compensated over time. This counterintuitive conclusion is justified by the fact that the intensity of the semimajor axis drift rate is inversely proportional to the square root of the semimajor axis itself. So, if the physical properties of the family members do not change with time, and in particular their rotation axis obliquities, the decrease of the semimajor axis is accelerated while the increase is decelerated. The resulting estimated ages diverge: the 'external' age $T_{\rm est+}$ tends to be underestimated while the 'internal' age $T_{\rm est-}$ is overestimated. However, it is very unlikely that this bias manifests

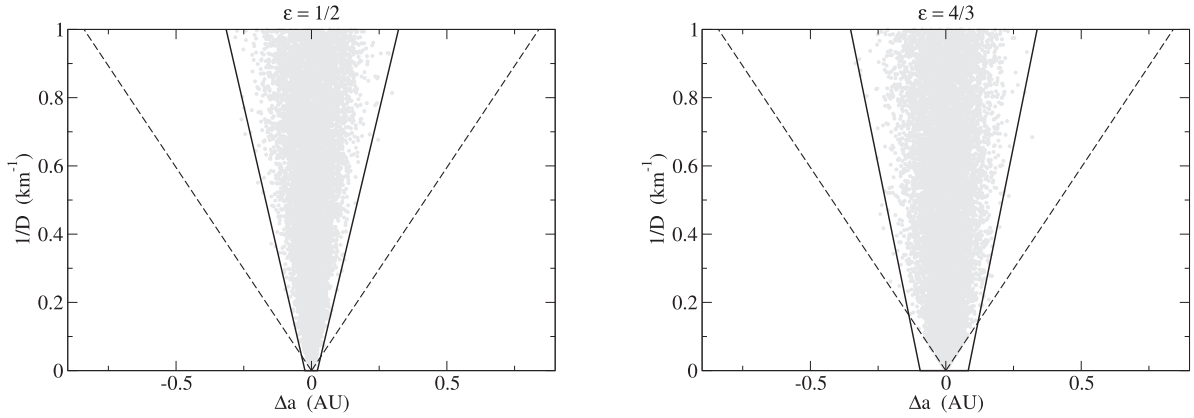

Figure 16. Final diagram (a, $1/D$) for a family after an evolution of 4 Gyr affected by the spin reset ($\epsilon = 1/2$ at left, $\epsilon = 4/3$ at right). Dashed lines represent the ideal positions of the V-shape borders if spin reset had been inactive, while solid lines represent the linear fit of the real borders.

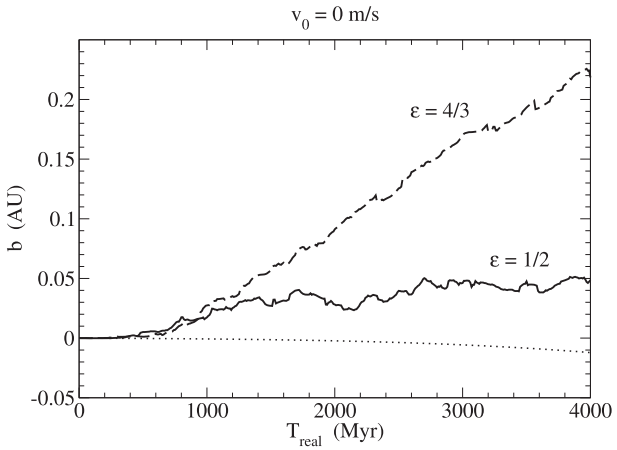

Figure 17. Value of the V-base versus $T_{\rm real}$ for an asteroid family affected by spin reset (solid line $\epsilon = 1/2$, dashed $\epsilon = 4/3$, dotted line: no spin reset).

itself as a systematic asymmetry of the ratio of the inverse slopes $|u_-|/u_+ > 1$ because the acceleration/deceleration mechanism affects the inverse slopes by 10 per cent at most.

An interesting feature of the V-shapes of the real asteroid families is that the V-bases tend to be systematically negative. Milani et al. (2014, 2019) suggested that this trend could be due to some correlations between the spin axis orientation and the ejection velocities of the family members. This explanation seems not to be supported by the results of our numerical experiments. Velocity–spin axis correlation produces positive or negative offset in age determination as discussed in Section 4.2. In particular, in the case of a negative correlation, the initial 'collapse' of the V-shape removes quickly the possible initial age bias introduced by the break-up velocity field, in other words resetting the age 'clock' of the asteroid family. Nevertheless, a velocity–spin axis correlation does not introduce an important systematic variation of the V-base. This is basically due to the fact that, assuming an exponent $\beta \sim 1$ in equation (2) linking size and ejection velocity, the expected borders of the V-shape in the plane $1/D$ versus a are more or less straight lines, and the Yarkovsky effect can only modify their inverse slopes but not their intersections with the horizontal axis.

Without abandoning the hypothesis $\beta \sim 1$, only two physical effects are able to change the curvature of the V-shape borders, and produce systematically non-zero V-base values: the gravitational reaccumulation during the primordial break-up process and the collisional spin axes re-orientation. As shown by the numerical simulations, the two mechanisms are competing. The gravitational reaccumulation produces an initially negative value of the V-base that is more and more amplified during the subsequent dynamical evolution. The spin reset tends to systematically increases the V-base towards positive values. The different impact of the two mechanisms derives from the different way they modify the geometry of the V-shape borders. The net result depends on the degree of reaccumulation and the age of the family. The spin reset is able to cancel out the effect of even the most severe reaccumulation in few hundred million years, producing distributions of the V-base with mean null or positive, not compatible with the observational evidence. A possible explanation is that the spin reset is not as efficient as it is thought. If the characteristic re-orientation time $\tau_{\rm rot,\,0}$ for $D_0 = 1$ km in equation (14) was much much longer, the spin reset would have effects on the V-base over much longer time-scales. On the other hand, if the exponent ϵ was smaller than 1/2 the differential effect of the spin reset on members of different sizes would be more limited. This would reduce the curvature of the V-shape border due to the spin reset and the V-base value as well. However, it is important to note that in the latter case the spin reset would still have important effects on the age determination for families older than 1 Gyr (Fig. 15).

We can argue that the YORP effect (Vokrouhlický et al. 2007) should not introduce substantial changes to the just described scenario. YORP torque changes very quickly the axis obliquity to the extreme values 0 or π, maximizing the Yarkovsky semimajor axis drift rate, with a characteristic time $\tau_{\rm yorp}$ proportional to the square of the asteroid size. This does not change the random walk nature of the mobility of the semimajor axes that reset their direction with a characteristic time $\tau_{\rm rot}$. In any case, the diffusion of the semimajor axes is proportional to the square root of the time. The difference between the two regimes $\tau_{\rm rot} \ll \tau_{\rm yorp}$ and $\tau_{\rm rot} \gg \tau_{\rm yorp}$ introduces a factor $\sim$2 in the diffusion speed. The case $\tau_{\rm rot} \gg \tau_{\rm yorp}$ is treated in our model not assuming a completely random direction of the spin axis after a collision reset but allowing only two possible values 0 and π for the obliquity (with equal probability). As expected, numerical tests confirmed that in this regime the diffusion is about twice faster than in the 'normal' one $\tau_{\rm rot} \ll \tau_{\rm yorp}$. The value of $\tau_{\rm yorp}$ is expected to be of the order of few millions of years for 1 km-sized objects. According to Fig. 3 it results that $\tau_{\rm rot} \gg \tau_{\rm yorp}$ practically throughout the size range if $\epsilon = 4/3$. Instead, if $\epsilon = 1/2$, the regime $\tau_{\rm rot} \gg$

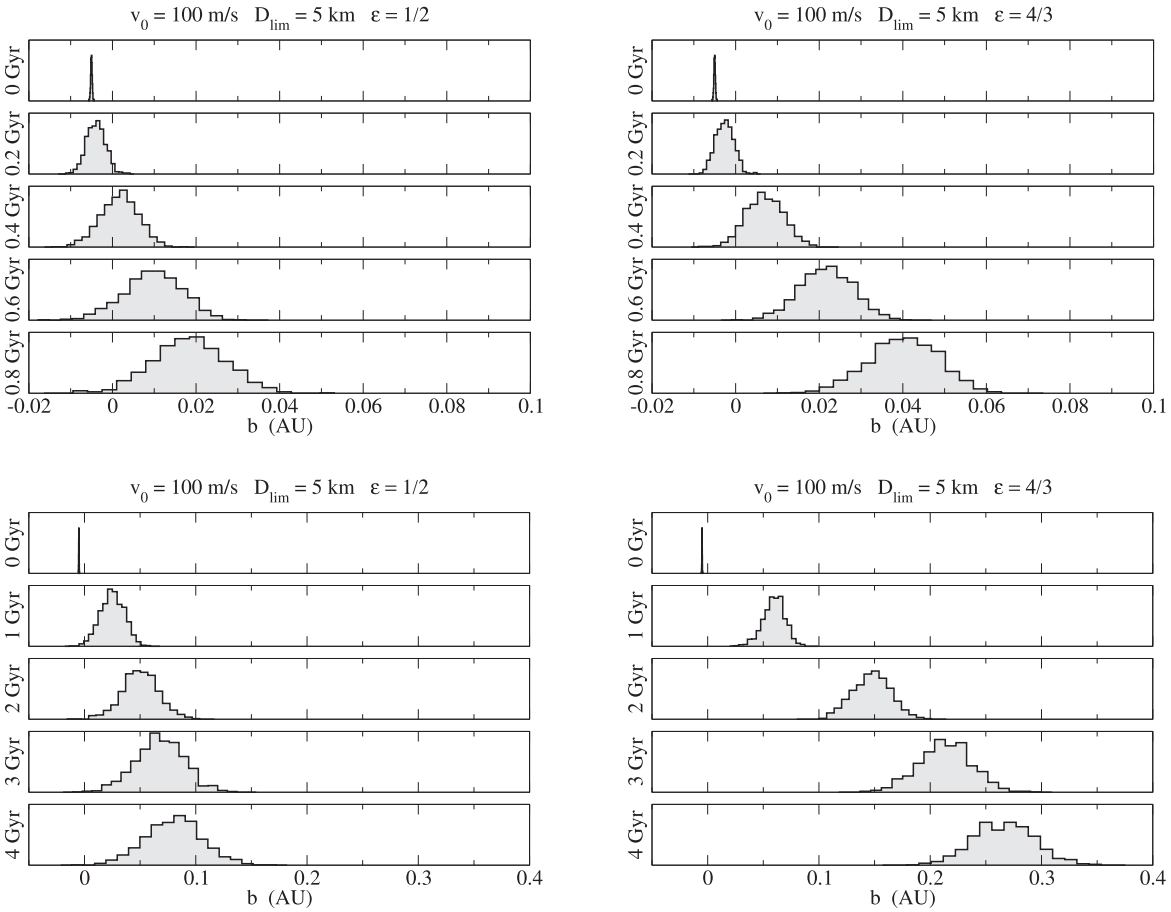

Figure 18. Evolution with time of the distribution of the V-base size b for a set of 1000 asteroid families affected by an initial reaccumulation and spin reset in the post-formation phase. The break-up parameters are $v_0 = 100$ m s^{-1} and $D_{\rm lim} = 5$ km. The exponent of the spin reset is $\epsilon = 1/2$ at left and 4/3 at right. Top: Evolution during the first 800 Myr. Bottom: Evolution up to 4 Gyr.

$\tau_{\rm yorp}$ would be typical of smaller objects (more or less below 10 km). This could entail a faster diffusion of the upper part of the V-shape (corresponding to the range of smaller objects), reducing the curvature of the borders and limiting in some way the increase of the V-base due to the spin reset. On the other hand, the high uncertainty on the value of $\tau_{\rm yorp}$ can easily modify such conclusions. Moreover, YORP torque does not only affect asteroid obliquities but also their rotation periods, pushing them towards the extreme conditions of very fast (potentially causing a mechanical disintegration of the body) or very slow rotation, until a tumbling rotational state. In both cases, the efficiency of the Yarkovsky semimajor axis mobility is reduced, increasing the bias in the determination of the age. This specific point deserves further investigation in future work.

ACKNOWLEDGEMENTS

The authors thank the referee Valerio Carruba for the useful and constructive comments.

DATA AVAILABILITY

The data generated from computations are reported in the paper, and any additional data will be made available upon reasonable request to the corresponding author.

REFERENCES

Bolin B. T., Delbo M., Morbidelli A., Walsh K. J., 2017, Icarus, 282, 290
Bolin B. T., Walsh K. J., Morbidelli A., Delbó M., 2018, MNRAS, 473, 3949
Bottke W. F., Vokrouhlický D., Broz M., Nesvorný D., Morbidelli A., 2001, Science, 294, 1693
Bottke W. F., Vokrouhlický D., Rubincam D. P., Broz M., 2002, in Bottke W. F., Cellino A., Paolicchi P., Binzel R. P., eds, Asteroids III. University of Arizona Press, Tucson, p. 395
Bottke W. F. et al., 2015, Icarus, 247, 191
Brouwer D., 1951, AJ, 56, 9
Brož M., Morbidelli A., 2013, Icarus, 223, 844
Čapek D., Vokrouhlický D., 2004, Icarus, 172, 526
Carruba V., Nesvorný D., Aljbaae S., 2016, Icarus, 271, 57
Carruba V., Vokrouhlický D., Novaković B., 2018, Planet. Space Sci., 157, 72
Cellino A., Michel P., Tanga P., Zappalà V., Paolicchi P., Dell'Oro A., 1999, Icarus, 141, 79
Cellino A., Dell'Oro A., Zappalà V., 2004, Planet. Space Sci., 52, 1075
Cotto-Figueroa D., Statler T. S., Richardson D. C., Tanga P., 2015, ApJ, 803, 25
D'Abramo G., Dell'Oro A., Paolicchi P., 1999, Planet. Space Sci., 47, 975
Dell'Oro A., Cellino A., 2007, MNRAS, 380, 399
Dell'Oro A., Paolicchi P., 1998, Icarus, 136, 328
Farinella P., Vokrouhlický D., 1999, Science, 283, 1507
Farinella P., Paolicchi P., Cellino A., Zappala V., 1988, Bull. Astron. Belgrade, 138, 88
Farinella P., Vokrouhlický D., Hartmann W. K., 1998, Icarus, 132, 378

Fujiwara A., Tsukamoto A., 1981, Icarus, 48, 329
Fujiwara A., Cerroni P., Davis D., Ryan E., Di Martino M., Holsapple K., Housen K., 1989, in Binzel R.P., Gehrels T., Matthews M.S., eds, Asteroids II. University of Arizona Press, Tucson, p. 240
Giblin I., Martelli G., Smith P. N., Cellino A., Di Martino M., Zappalà V., Farinella P., Paolicchi P., 1994, Icarus, 110, 203
Golubov O., Krugly Y. N., 2012, ApJ, 752, L11
Harris A. W., 1979, Icarus, 40, 145
Holsapple K., Giblin I., Housen K., Nakamura A., Ryan E., 2002, in Bottke W.F., Cellino A., Paolicchi P., Binzel R.P., eds, Asteroids III. University of Arizona Press, Tucson, p. 443
Kadono T., Arakawa M., Ito T., Ohtsuki K., 2009, Icarus, 200, 694
Knežević Z., Milani A., 2000, Celest. Mech. Dyn. Astron., 78, 17
Knežević Z., Milani A., 2003, A&A, 403, 1165
Marzari F., Rossi A., Golubov O., Scheeres D. J., 2020, AJ, 160, 128
Milani A., Cellino A., Knežević Z., Novaković B., Spoto F., Paolicchi P., 2014, Icarus, 239, 46
Milani A., Knežević Z., Spoto F., Paolicchi P., 2019, A&A, 622, A47
Murray C. D., Dermott S. F., 1999, Solar System Dynamics. Cambridge University Press, Cambridge
Nesvorný D., Bottke W. F., Jr, Dones L., Levison H. F., 2002, Nature, 417, 720
O'Brien D. P., Greenberg R., 2005, Icarus, 178, 179
Paolicchi P., Knežević Z., 2016, Icarus, 274, 314
Paolicchi P., Cellino A., Farinella P., Zappalà V., 1989, Icarus, 77, 187
Paolicchi P., Verlicchi A., Cellino A., 1996, Icarus, 121, 126
Petit J.-M., Farinella P., 1993, Celest. Mech. Dyn. Astron., 57, 1
Rubincam D. P., 2000, Icarus, 148, 2
Ševeček P., Brovz M., Čapek D., Ďurech J., 2015, MNRAS, 450, 2104
Spoto F., Milani A., Knezevic Z., 2015, Icarus, 257, 275
Statler T. S., 2009, Icarus, 202, 502
Vokrouhlický D., 1999, A&A, 344, 362
Vokrouhlický D., Brož M., Bottke W. F., Nesvorný D., Morbidelli A., 2006a, Icarus, 182, 118
Vokrouhlicky D., Broz M., Bottke W. F., Nesvorny D., Morbidelli A., 2006b, Icarus, 183, 349
Vokrouhlický D., Breiter S., Nesvorný D., Bottke W. F., 2007, Icarus, 191, 636
Zappalà V., Cellino A., Dell'Oro A., Migliorini F., Paolicchi P., 1996, Icarus, 124, 156

APPENDIX A: POLARIZED SPIN–VELOCITY GEOMETRY

The case of correlation between initial position in V-shape diagram and Yarkovsky drift direction discussed in Section 4.2 arises from the geometric condition $\boldsymbol{s} \propto (\boldsymbol{k} \times \boldsymbol{v})$ characterizing the spin–velocity field in this particular case, where $\boldsymbol{k}$ is the cylindrical symmetry axis of the field, $\boldsymbol{v}$ is the ejection velocity, and $\boldsymbol{s}$ the spin of the fragment. In other words, the spin is bound to be orthogonal to the plane containing $\boldsymbol{k}$ and $\boldsymbol{v}$. In terms of the parameters of the model described in Section 2.1, the condition $\boldsymbol{s} \propto (\boldsymbol{k} \times \boldsymbol{v})$ corresponds to the values $\theta_h = 0$ and $\eta_s = 0$ (Fig. 1). The direction of the velocity $\boldsymbol{v}$ is assumed to be totally free and isotropic ($\eta_v = \pi$).

According to the orientation of the vector $\boldsymbol{k}$ with respect to the Gauss comoving orthonormal basis $\boldsymbol{R}$ (radial), $\boldsymbol{T}$ (transverse), and $\boldsymbol{N}$ (normal to the orbit plane, see Murray & Dermott 1999), different kind of correlations between the component of $\mathbf{s}$ along $\boldsymbol{N}$ (determining the magnitude and direction of the Yarkovsky drift rate) and the component of $\boldsymbol{v}$ along $\boldsymbol{T}$ (on which the difference between the fragment's and parent body's semimajor axis depends) appear.

Neglecting their magnitude and focusing on the relative orientations of the involved vectors only, hereinafter any vector in this Appendix is assumed to be a unit vector.

By definition, the three versors of the Gauss basis fulfill the following conditions:

$$\boldsymbol{R} \times \boldsymbol{T} = \boldsymbol{N}$$

$$\boldsymbol{T} \times \boldsymbol{N} = \boldsymbol{R}$$

$$\boldsymbol{N} \times \boldsymbol{R} = \boldsymbol{T}$$

Let $\boldsymbol{V}$ be the velocity unit vector:

$$\boldsymbol{V} = V_R \boldsymbol{R} + V_T \boldsymbol{T} + V_N \boldsymbol{N}$$

with

$$V_R^2 + V_T^2 + V_N^2 = 1.$$

Following the hypothesis of isotropy of $\boldsymbol{V}$, we have

$$\langle V_R \rangle = \langle V_T \rangle = \langle V_N \rangle = 0$$

$$\langle V_R^2 \rangle = \langle V_T^2 \rangle = \langle V_N^2 \rangle = \frac{1}{3}$$

$$\langle V_R V_T \rangle = \langle V_R V_N \rangle = \langle V_T V_N \rangle = 0,$$

where $\langle\rangle$ represents the average operation over all randomly generated fragments.

By construction, the spin unit vector $\boldsymbol{S}$ is

$$\boldsymbol{S} = \frac{\boldsymbol{K} \times \boldsymbol{V}}{|\boldsymbol{K} \times \boldsymbol{V}|},$$

where $\boldsymbol{K}$ is the cylindrical symmetry axis of the field, and in terms of Gauss components:

$$\boldsymbol{S} = S_R \boldsymbol{R} + S_T \boldsymbol{T} + S_N \boldsymbol{N}.$$

We are interested in the relationship between $S_N = \boldsymbol{S} \cdot \boldsymbol{N}$ (normal spin component) and $V_T = \boldsymbol{V} \cdot \boldsymbol{T}$ (transverse ejection velocity component). In particular, we want to evaluate the correlation:

$$\sigma_{NT} = \langle S_N V_T \rangle - \langle S_N \rangle \langle V_T \rangle$$

It is important to note that, like $\boldsymbol{V}$, also for the spin $\langle \boldsymbol{S} \rangle = \boldsymbol{0}$, because for a fragment with velocity $\boldsymbol{V}$ another one with velocity $-\boldsymbol{V}$ can exist with the same probability, and the corresponding spin is $-\boldsymbol{S}$. In particular $\langle S_N \rangle = 0$. So:

$$\sigma_{NT} = \langle S_N V_T \rangle$$

Regarding the orientation of the symmetry axis $\boldsymbol{K}$, three important extreme cases exist.

If $\boldsymbol{K} = \boldsymbol{N}$ (impact direction parallel to the normal axis of the parent body orbit):

$$S_N = \frac{\boldsymbol{N} \cdot (\boldsymbol{N} \times \boldsymbol{V})}{|\boldsymbol{N} \times \boldsymbol{V}|}$$

that is

$$S_N = 0 \qquad (\boldsymbol{K} = \boldsymbol{N}). \tag{A1}$$

In this case, the spin vector has no normal component, whatever the value of V_T is (Fig. A1, top left). It is evident that $\sigma_{NT} = 0$.

If $\boldsymbol{K} = \boldsymbol{T}$ (impact along the orbital motion):

$$S_N = \frac{\boldsymbol{N} \cdot (\boldsymbol{T} \times \boldsymbol{V})}{|\boldsymbol{T} \times \boldsymbol{V}|} = \frac{\boldsymbol{V} \cdot (\boldsymbol{N} \times \boldsymbol{T})}{|\boldsymbol{T} \times \boldsymbol{V}|}$$

but $\boldsymbol{N} \times \boldsymbol{T} = -\boldsymbol{R}$, and:

$$\boldsymbol{T} \times \boldsymbol{V} = -V_R \boldsymbol{N} + V_N \boldsymbol{R}$$

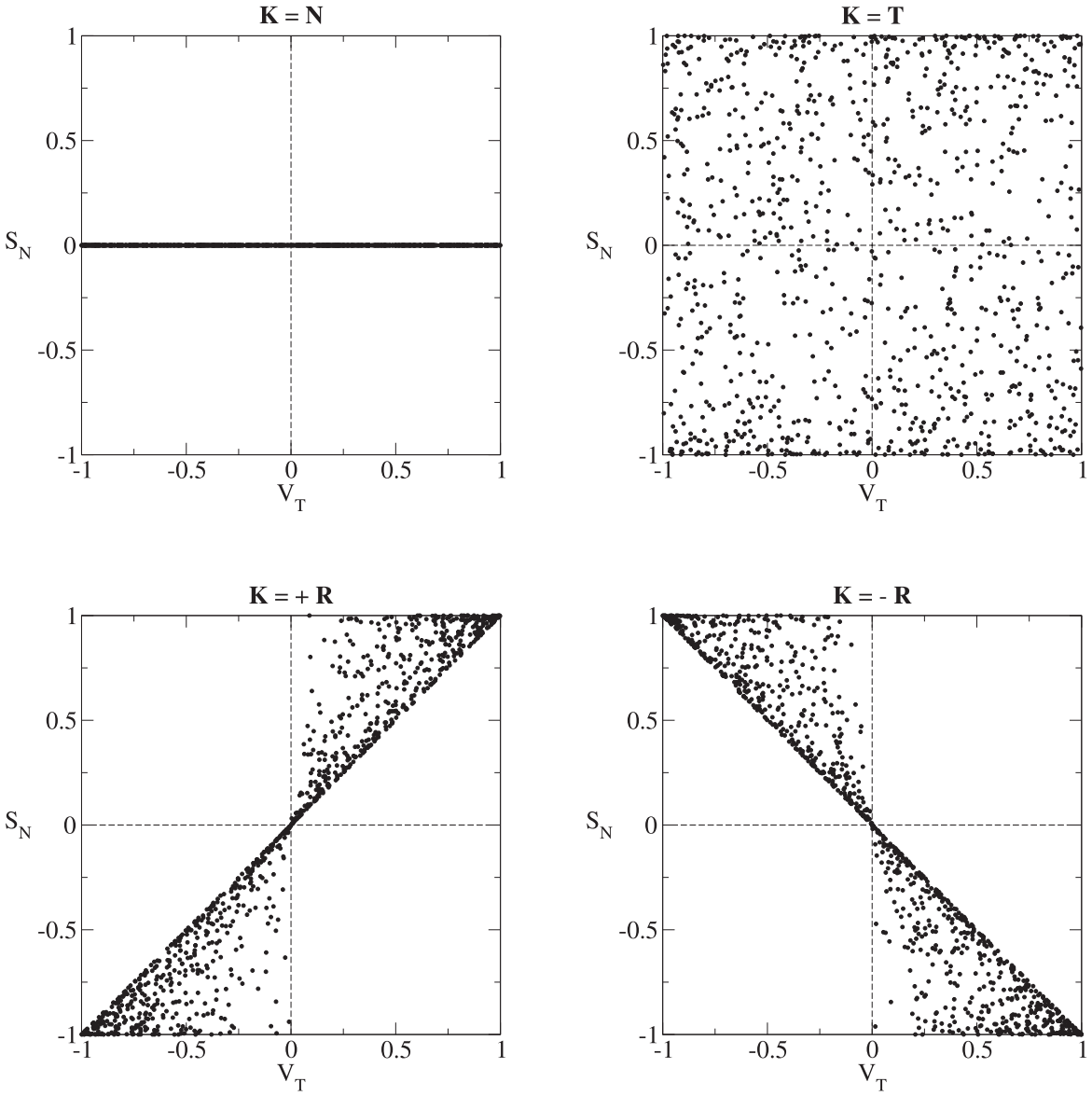

Figure A1. Component of the spin axis unit vector normal to orbit plane (cosine of the spin axis obliquity) versus transverse component of the ejection velocity unit vector for a simulated break-up according to the model described in Section 2.1 with parameters $\theta_h = 0$ and $\eta_s = 0$. Each point represents a single fragment. $\boldsymbol{K}$ is the symmetry axis of the spin–velocity field.

so that:

$$S_N = -\frac{V_R}{\sqrt{V_R^2 + V_N^2}} \qquad (\boldsymbol{K} = \boldsymbol{T}). \tag{A2}$$

In this case:

$$\sigma_{NT} = -\langle \frac{V_R V_T}{\sqrt{1 - V_T^2}} \rangle$$

For a fragment with components (V_R, V_T), we can find with equal chance three other fragments with components (V_R, $-V_T$), ($-V_R$, V_T), and ($-V_R$, $-V_T$). In any case the sum of the corresponding four terms in the average is zero. Also in this case no correlation between S_N and V_T exists (Fig. A1, top right). The same conclusion holds also if $\boldsymbol{K} = -\boldsymbol{T}$.

The last case regards an impact along the radial direction. It consists of two subcases, according to the direction of the impact. If $\boldsymbol{K} = \boldsymbol{R}$:

$$S_N = \frac{\boldsymbol{N} \cdot (\boldsymbol{R} \times \boldsymbol{V})}{|\boldsymbol{R} \times \boldsymbol{V}|} = \frac{\boldsymbol{V} \cdot (\boldsymbol{N} \times \boldsymbol{R})}{|\boldsymbol{R} \times \boldsymbol{V}|}$$

and taking into account that:

$$\boldsymbol{R} \times \boldsymbol{V} = V_T \boldsymbol{N} - V_N \boldsymbol{T}$$

we have

$$S_N = \frac{V_T}{\sqrt{V_T^2 + V_N^2}} \qquad (\boldsymbol{K} = \boldsymbol{R}). \tag{A3}$$

In this case, the correlation is

$$\sigma_{NT} = \langle \frac{V_T^2}{\sqrt{1 - V_R^2}} \rangle.$$

In this case simply σ_{NT} is the sum of positive terms alone entailing $\sigma_{NT} > 0$. A **positive** correlation between S_N and V_T exists: fragments

ejected with $V_T > 0$ (entailing an initial orbital semimajor axis larger than the parent body's one) are characterized by a Yarkovsky drift producing a semimajor axis **increasing** ($S_N > 0$) and *vice versa* (Fig. A1, bottom left).

On the contrary, if $\boldsymbol{K} = -\boldsymbol{R}$:

$$S_N = -\frac{V_T}{\sqrt{V_T^2 + V_N^2}} \qquad (\boldsymbol{K} = -\boldsymbol{R}) \tag{A4}$$

a **negative** correlation between S_N and V_T exists: fragments ejected with $V_T > 0$ are characterized by a Yarkovsky drift producing a semimajor axis **decreasing** ($S_N < 0$) and *vice versa* (Fig. A1, bottom right).

Finally, again for $\boldsymbol{K} = \pm\boldsymbol{R}$, because $V_T^2 + V_N^2 \leq 1$, it follows that $|S_N/V_T| \geq 1$, as shown in Fig. A1 at the bottom.

The different types of correlation between the normal component S_N of the spin axis unit vector and the transverse component V_T of the ejection velocity unit vector shown in Fig. A1 can be easily translated in terms of correlation between the cosine of the obliquity ϕ and the difference Δa between the semimajor axis of the fragment and the parent body shown in Fig. 9. The different distribution of the points for the case $\boldsymbol{k} = \boldsymbol{T}$, uniform in Fig. A1 but not in Fig. 9, is simply due to the fact that in the former case $|\boldsymbol{V}| = 1$ for all fragments, while in the second case the magnitude of the velocity depends on the diameter of the fragment through equations (1) and (2). Moreover in the case $\boldsymbol{k} = \pm\boldsymbol{R}$, we have seen that if $V_T = 0$ it follows that $S_N = 0$ too. On the other hand, $V_T = 0$ entails $\Delta a = 0$ but, depending on the values of the component V_N, the final orbit has values of inclination and longitude of the node different from these orbit does not coincide with $\boldsymbol{N}$, that is the axis of the parent body orbit. This is the reason for the slight dispersion of the points around $\Delta a = 0$ in Fig. 9 at the bottom.

APPENDIX B: INITIAL V-SHAPE BOUNDARY FOR ISOTROPIC EJECTION FIELDS

At the beginning, just after the complete dispersion of the parent body fragments, the difference Δa between the semimajor axis of the orbit of an ejected fragment and the semimajor axis of the parent body's orbit can be evaluated with good approximation according to the zero-order Gauss' formula:

$$\Delta a = \frac{2}{n}\Delta T,$$

where n is the parent body orbital mean motion and ΔT is the transverse component of the fragment ejection velocity at infinity, that is after the ballistic phase during which the motion of the fragments is mainly affected by their mutual gravity.

We assume that the fragments are ejected isotropically with velocity $V_{\rm ej}$ strictly dependent on their diameter as

$$V_{\rm ej} = kD^{-\beta}.$$

Moreover, we assume that, statistically, the effect of the mutual gravitational attraction of the fragments is to reduce the magnitude of the velocity, so that their velocity at infinity is

$$V_\infty = \sqrt{V_{\rm ej}^2 - V_{\rm esc}^2},$$

where $V_{\rm esc}$ is the effective escape velocity. It is not important here what is the exact meaning and value of $V_{\rm esc}$. In this simplified picture, we assume only that such a single parameter exists describing the mutual gravitational field and reaccumulation according to equation (3).

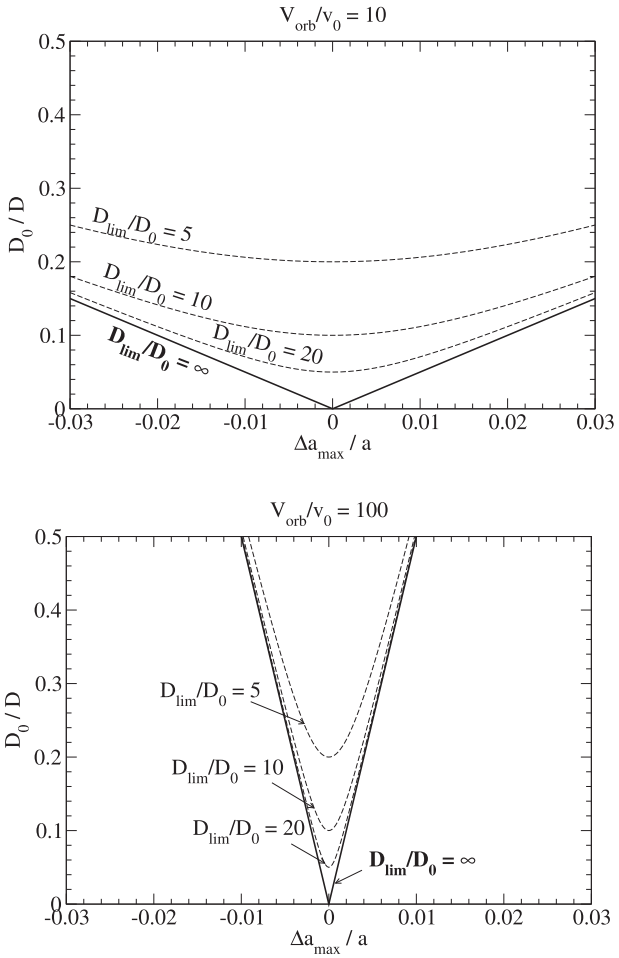

Figure B1. Examples of V-shape ideal borders for isotropic asteroid families with $\beta = 1$, represented in the plane D_0/D versus $\Delta a_{\rm max}/a$.

Hence, for a given value D of the fragment diameter, the maximum value of the transverse component of the velocity field at infinity is

$$\Delta T_{\rm max} = V_\infty = \sqrt{k^2 D^{-2\beta} - V_{\rm esc}^2}$$

and, accordingly, for a given D the maximum Δa in the family is

$$\Delta a_{\rm max} = \frac{2}{n}\Delta T_{\rm max}$$

from which

$$\frac{1}{D} = k^{-1/\beta}\left[\frac{n^2}{4}\Delta a_{\rm max}^2 + V_{\rm esc}^2\right]^{1/(2\beta)}.$$

Thus, in this simplified model, the curve $(\Delta a_{\rm max}, 1/D)$ cannot reach the abscissa axis $\Delta a_{\rm max}$ if $V_{\rm esc} \neq 0$. The minimum possible value of $(1/D)$ is

$$\left(\frac{1}{D}\right)_{\rm lim} = \left(\frac{V_{\rm esc}}{k}\right)^{1/\beta}$$

excluding the reaccumulated largest remnant with a final orbit close to the parent body's one.

Following the formulas of our model described in Section 2.1:

$$k = v_0 D_0^\beta$$

and recalling that

$$n^2 a^3 = GM_*,$$

where G is the universal gravitational constant, M_* is the mass of the Sun, and a is the semimajor axis of the orbit of the parent body, it follows that

$$\frac{D_0}{D_{\rm lim}} = \left(\frac{V_{\rm esc}}{v_0}\right)^{1/\beta}$$

$$\frac{D_0}{D} = \left[\frac{1}{4}\left(\frac{V_{\rm orb}}{v_0}\right)^2\left(\frac{\Delta a_{\rm max}}{a}\right)^2 + \left(\frac{D_0}{D_{\rm lim}}\right)^{2\beta}\right]^{1/(2\beta)}, \qquad \text{(B1)}$$

where

$$V_{\rm orb}^2 = \frac{GM_*}{a}$$

is the mean orbital velocity of the parent body.

In conclusion, in the case of an isotropic ejection velocity field and a gravitational reaccumulation according to the assumptions discussed in Section 2.1, the initial V-shape border, in the plane D_0/D versus $\Delta a_{\rm max}/a$, is a curve described by equation (B1). In the case $\beta = 1$ the V-shape is a hyperbole, as in the examples shown in Fig. B1.

This paper has been typeset from a TEX/LATEX file prepared by the author.